

Bright 22 μm Excess Candidates from WISE All-Sky Catalog and Hipparcos Main Catalog

Chao-Jian Wu^{1,2,3}, Hong Wu^{1,3}, Man-I Lam^{1,3}, Ming Yang^{1,3}, Xiao-Qing Wen³, Shuo Li⁴,
Tong-Jie Zhang², & Liang Gao¹

ABSTRACT

In this paper we present a catalog which includes 141 bright candidates (≤ 10.27 mag, V band) showing the infrared (IR) excess at 22 μm . Of which, 38 stars are known IR excess stars or disk, 23 stars are double or multiple stars and 4 are Be stars. While the remaining more than 70 stars are identified as the 22 μm excess candidates in our work. The criterion of selecting candidates is $K_s - [22]_{\mu\text{m}}$. All these candidates are selected from *WISE* All-sky data cross-correlated with *Hipparcos* Main Catalog and the likelihood-ratio technique is employed. Considering the effect of background, we introduce the *IRAS* 100 μm level to exclude the high background. We also estimated the coincidence probability of these sources. In addition, we presented the optical to mid-infrared SEDs and optical images of all the candidates, and gave the observed optical spectra of 6 stars with NAOC's 2.16-m telescope. To measure for the dust amount around each star, the fractional luminosity is also provided. We also test whether our method of selecting IR excess stars can be used to search for extra-solar planets, we cross-matched our catalog with known IR-excess stars having planets but none is matched. Finally, we give the fraction of stars showing IR-excess for different spectral type of main-sequence stars.

Subject headings: infrared: stars-planetary systems - stars: formation - planetary systems: protoplanetary disks

¹National Astronomical Observatories, Chinese Academy of Sciences, Beijing 100012, P.R. China

²Department of Astronomy, Beijing Normal University, Beijing, 100875, P. R. China

³Key Laboratory of Optical Astronomy, National Astronomical Observatories, Chinese Academy of Sciences, Beijing 100012, P.R. China

⁴Department of Astronomy, Peking University, Beijing, 100871, P. R. China

1. INTRODUCTION

The nature of IR excess is still uncertain: it may be produced by protostars (Thompson 1982) or the surrounding dust disk (Gorlova et al. 2004, 2006; Rhee et al. 2007; Hovhannisyan et al. 2009; Koerner et al. 2010; Wu et al. 2012), or from giant stars, and it may also be due to M dwarfs, brown dwarfs (Debes et al. 2011). However, the IR excess could also come from the companion star, background galaxy, background nebula or interstellar medium or random foreground object, not from the object itself (Ribas et al. 2012).

Since the first discovery of the debris disk around Vega by infrared excess, (Aumann et al. 1984), IR excess is a useful tool to search debris disk. To date, many works on searching for stars with IR excess emission have been conducted. Most of the samples used in the previous work were selected from *IRAS*, *Infrared Space Observatory (ISO)* and *Spitzer Space Telescope* (Rhee et al. 2007; Lagrange et al. 2000; Zuckerman 2001; Decin et al. 2003), and the searching wavelength was focused at 60 μm or 70 μm . E.g., Rhee et al. (2007) identified 146 stars that show the excess emission at 60 μm by cross-correlating *IRAS* catalogs with *Hipparcos* stars, and 33 stars were found to have debris disks. In addition, several other papers published between 2004 and 2005 reported that many Vega-like stars detected by *Spitzer* at 70 μm have not been detected at 60 μm by *IRAS* and *ISO* (Meyer et al. 2004; Chen et al. 2005b; Beichman et al. 2005; Low et al. 2005; Kim et al. 2005).

Some works were also done at shorter wavelengths, e.g., 24 μm . Especially after the launch of the *Spitzer* Space Telescope (Werner et al. 2004), many *Spitzer* sub-programs were carried out. For example, some wide-field surveys from the Multi-band Imaging Photometer (MIPS) (Rieke et al. 2004) were performed at three mid-to-far infrared bands (24, 70 and 160 μm). Many stars with 24 μm excess are studied using the MIPS's 24 μm database. Low et al. (2005) found 4 out of 24 stars in the 810 Myr old TW Hya association shows 24 μm excess. Young et al. (2004) found several stars with 24 μm excess from the cluster NGC 2547. Gorlova et al. (2004, 2006) found stars with 24 μm excess from the open cluster M47 and Pleiades cluster using the selection criterion $K_S - [24]_{vega} \geq 0.44$. Su et al. (2006) reported that the 24 μm excess occurrence rate is about 32% by studying 160 A-type main-sequence stars. At high galactic latitudes, Wu et al. (2012) found eleven 24 μm excess stars with older age.

With the release of the Wide-field Infrared Survey Explorer (WISE; Wright et al. 2010) all sky data, the observations at 22 μm will undoubtedly provide an opportunity to search for more IR excess stars in the whole sky (Wu et al. 2012). Some related work have been published. Kennedy & Wyatt (2012) described a search for IR excess stars from *Kepler* and *WISE* and concluded that the excesses in the *Kepler* field are mainly due to high background level. Lawler & Gladman (2012) studied the dust emission around more than

900 *Kepler* exoplanet candidates using *WISE* data and they found 8 candidates with IR excess. Morales et al. (2012) studied the dust of 591 planetary systems from Exoplanet Encyclopaedia as of 2012 January 31, 350 can be detected by *WISE* and 9 stars have mid-IR excess. Avenhaus et al. (2012) searched IR excess mainly for M stars. In our work, we focus on the bright stars and the observed information at $22\mu\text{m}$. More information about WISE will be described in Section 2.1.

In order to study the properties of the IR excess stars in more detail, the information of WISE is not enough, and we need more observed quantities, e.g., optical data, distance, spectral type and so on. So we choose the *Hipparcos* Main Catalog for cross-correlating with WISE due to its highest photometric precision and distance information. The *Hipparcos* Catalog, one of the two major stellar catalogs resulting from the ESAs *Hipparcos* space astrometry project, was completed in August 1996, and published in June 1997 (ESA 1997). In Section 2.2, detailed information of *Hipparcos* are presented and the reason of only using the *Hipparcos* Main Catalog is also explained.

In the previous study, similar works were purely based on the *WISE* and SDSS DR7 (Debes et al. 2011) or *IRAS* and *Hipparcos* catalogs (Rhee et al. 2007). In this work, we firstly use the all-sky WISE data to search for bright IR excess stars by matching with *Hipparcos* Catalog. Generally, color-color diagram is a useful tool for detecting IR excess (Hoard et al. 2007; Wellhouse et al. 2005; Wachter et al. 2003).

In this paper, we describe the *WISE* all sky data, *Hipparcos* Catalog, candidate selection criterion, source identification method and optical observations in Section 2. In Section 3, we classified the IR excess stars, analyzed their infrared properties of and presented their spectral energy distributions (SEDs) and the optical images. The conclusion and summary are presented in Section 4.

2. CANDIDATES SELECTION AND OBSERVATIONS

2.1. WISE All-Sky Catalog

The WISE satellite was launched on December 14, 2009. It mapped the sky at 3.4, 4.6, 12, and $22\mu\text{m}$ (W1, W2, W3, W4) with an angular resolution of $6''.1$, $6''.4$, $6''.5$, and $12''.0$ in the four bands, respectively, achieving 5σ point source sensitivities better than 0.08, 0.11, 1 and 6 mJy in the four bands in unconfused regions on the ecliptic plane (Wright et al. 2010). The all-sky data were released on March 14th 2012 and it includes all the data taken during the WISE full cryogenic mission phase, from January 7th 2010 to August 6th 2010, which were processed with improved calibrations and reduction algorithms. Released

data products include an Atlas of 18,240 image sets, a source catalog containing positional and photometric information for over 563 million objects detected on the WISE images. It supersedes the Preliminary Data which was released in April, 2011¹. The mission of *WISE* has several main goals, such as taking a census of cool stars and brown dwarfs close to the Sun, probing the dustiest galaxies in the universe, and cataloging the Near Earth Object population (Wright et al. 2010; Debes et al. 2011). It will also provide crucial information on the IR sky at a sensitivity 100 times better than that of *IRAS*. However, the WISE team found an overestimate in brightness in the 4.6 μm (W2) band² and the bias can be reach nearly 1 mag (Tisserand 2012). In our work, we also found the existence of the bias on bright sources at 4.6 μm band. It will be described in Section 3.3.

In this paper, we firstly selected the all-sky sources from the WISE All-Sky data catalog with the criterion $S/N \geq 20$ at W4 (22 μm) band, they contain positional and photometric information including J, H, K_s bands of 2MASS and 3.4, 4.6, 12, and 22 μm bands (W1, W2, W3, W4) of WISE. After filtering with this criterion we obtained a catalog with 971,148 sources. In the next step, it will be used to cross-correlated with the *Hipparcos* Main Catalog.

2.2. Hipparcos Main Catalog

ESA’s Hipparcos space astrometry mission was a pioneering European project. It was launched in August 1989 and has successfully observed the celestial sphere for 3.5 years before the operation was ceased in March 1993, and its scientific goal was to provide positions, proper motions, and direct distance of stars near the solar system in order to study the physical properties, stellar structure and evolution of stars (Perryman et al. 1997, 1995). The *Hipparcos* Main catalog was generated from these observations by the main instrument and it includes 118,218 stars charted with the highest precision. Also, an auxiliary star mapper scanned many more stars with lesser accuracy, which was included in the Tycho Catalog with 1,058,332 stars. The Tycho 2 Catalog, completed in 2000, brings the total to 2,539,913 stars, and most of sources are bright stars with an apparent magnitude of 11. It provides the information on the position, proper motion and direct distance estimate for over 100,000 stars in the solar neighborhood (Perryman et al. 1997). So many observed parameters of stars in Hipparcos Catalog provide us enough information to study their physical characteristics. In this work, we used only the *Hipparcos* Main Catalog because of its highest precision. Meanwhile, it provided trigonometric parallaxes and proper motions

¹<http://wise2.ipac.caltech.edu/docs/release/allsky/>

²http://wise2.ipac.caltech.edu/docs/release/allsky/expsup/sec6_3c.html

for more than 100,000 stars with errors 1~2 mas.

2.3. Cross-Correlation

As described in the sections above, we cross-correlated the selected WISE sources with the *Hipparcos* Main Catalog. The matching radius we used here is $6''$, which is consistent with the Full-Width-at-Half-Maximum (FWHM) of the WISE’s PSF at $3.4 \mu\text{m}$ (Wright et al. 2010). The cross-matched catalog was obtained, and it contains about 66,667 sources. But these sources can’t be used directly. They should be filtered with full WISE and 2MASS photometric information. Moreover, we also select the *Hipparcos* sources with threshold $\delta_{plx} < 0.1$ meaning distance accuracy should be better than 10% and with a photometric error $\delta_{B-V} < 0.025$ (Perryman et al. 1995). Moreover, we should delete those saturation sources at K_s , $W3$ and $W4$ band. In fact, the photometric error at K_s band should also be noted, because K_s will be used as the criterion of selecting IR excess. To ensure the statistical accuracy (See Section 2.4), only those with $\sigma \leq 0.1$ at K_s band are selected. That is to say, 7,624 sources are used to search IR excess stars in our work.

2.4. Candidates Selection

2.4.1. $K_s - [22]$ Criterion

In this section, we will describe how to identify the IR excess candidates from the 7,624 samples (black dots in Figure 1). They all contains multi-band information, e.g., parallax value, spectral type and so on. Once we find the IR excess stars from the cross-correlated catalog, we can make a detailed study to the selected sources with so much observational information.

Gorlova et al. (2004, 2006) provided an approach on searching for IR excess in the mid-infrared band, and they used the criterion that the mean $K_s - [24]_{vega}$ (here $[24]$ means the vega magnitude at $24 \mu\text{m}$, $[22]$ has the same meaning) value should be greater than 0.33 at a 3σ confidence level ($0.33 = 3 \times 0.11$, where 0.11 is the 1σ value). While in Hovhannisyan et al. (2009), the criterion was changed slightly to be $K_s - [22] \geq 0.2$, but in this paper, there is an assumption that all the stars have $K_s - [24] = 0$. However, this assumption is invalid for our sources. WISE team shows that there is calibration offset relative to 2MASS K-band, in other word, the WISE-K color is not zero. So we have to redefined the criterion. Similar to Gorlova et al. (2004), the histogram of $K_s - [22]$ can help us to define the criterion. From Figure 2, we can see that the points along y axis show different scatter. So we divided

our samples into four parts to do statistics following $J - H \leq 0.1$, $0.1 < J - H \leq 0.3$, $0.3 < J - H \leq 0.5$ and $J - H > 0.5$, respectively. The results are shown in Figure 3, Figure 4, Figure 5, and Figure 6. The histogram of $K_s - [22]$ colors can be described by a Gaussian centered at $K_s - [22] = 0.015$ mag with $\sigma = 0.062$ mag for $J - H \leq 0.1$, $K_s - [22] = 0.045$ mag with $\sigma = 0.041$ mag for $0.1 < J - H \leq 0.3$, $K_s - [22] = 0.062$ mag with $\sigma = 0.039$ mag for $0.3 < J - H \leq 0.5$ and $K_s - [22] = 0.086$ with $\sigma = 0.034$ mag for $J - H > 0.5$ sources, respectively. We therefore define IR excess stars as those lying redward of $K_s - [22] = 0.015 + 4\sigma = 0.26$ for $J - H \leq 0.1$, $K_s - [22] = 0.045 + 4\sigma = 0.21$ for $0.1 < J - H \leq 0.3$, $K_s - [22] = 0.062 + 4\sigma = 0.22$ for $0.3 < J - H \leq 0.5$ and $K_s - [22] = 0.086 + 4\sigma = 0.22$ for $J - H > 0.5$. As shown in Figure 2, 495 sources (those locate at the right side of red dotted line) have $22 \mu\text{m}$ excess by using our criterion.

However, the 495 sources can not be identified as really IR excess stars. The excess may be from nearby bright stars or background. So we introduce another two criterion to exclude the fake candidates.

2.4.2. Likelihood Ratio

We used the likelihood-ratio (LR) technique to identify the WISE IR excess sources. Its principle is to accept the nearest optical source. The LR method was first used by Richter (1975) and defined as in Sutherland & Saunders (1992):

$$L = \frac{q(m)f(r)}{n(m)} \quad (1)$$

where $f(r)$ is the radial probability distribution function of the positional errors with separation in arcseconds r , given by Smith et al. (2011)

$$f(r) = \frac{1}{2\pi\sigma_{pos}^2} \exp(-r^2/2\pi\sigma_{pos}^2) \quad (2)$$

in which σ_{pos} is the uncertainty for the position, while $n(m)$ and $q(m)$ correspond to the surface density per magnitude and the probability distribution function, respectively.

In this work, for a WISE candidate with a magnitude of m (V mag from *Hipparcos*) at an angular separation r from a given optical source, the LR is dened as the ratio of the probability of the WISE object being the true counterpart of the optical source (Ciliegi et al. 2003). We assume that the probability distribution of angular separations follows a Gaussian distribution, as given by Sutherland & Saunders (1992), we can rewrite the LR as:

$$L = \frac{Q(\leq m_i) \exp(-r^2/2)}{2\pi\sigma_{pos}^2 n(\leq m_i)} \quad (3)$$

$Q(m)$ is the expected magnitude distribution of counterparts. It is given by

$$Q = \int_{-\infty}^{m_{lim}} q(m) dm \quad (4)$$

Generally, the positional uncertainty should depend on the signal-to-noise ratio (S/N) and on the FWHM. So we use the results derived by Ivison et al. (2007), which gave

$$\sigma_{pos} = 0.6 \frac{\text{FWHM}}{S/N} \quad (5)$$

Given LR, so we can define the reliability R_i for the i th counterpart again following Sutherland & Saunders (1992):

$$R_i = \frac{L_i}{\sum_i L_i + (1 - Q)} \quad (6)$$

where Q stands for the probability that the counterpart of the source is above the limiting magnitude. In Mainieri et al. (2008), they pointed out that values of Q in the range 0.5-1.0 will make no significant difference in the results. So we also choose $Q = 0.8$ in this work. We used equation 6 to calculate the reliability of all candidates and then we select those sources with reliability $R \geq 0.8$ and leave 378 sources in the IR excess catalog from Section 2.4. The reliability distribution of these sources is shown in Figure 7.

2.4.3. The Contamination of Background

With the parallax value provided by *Hipparcos*, the distance distribution is shown in Figure 8. The distance of a star is a very important parameter. Not only it can be used for luminosity classification, but it can be used to determine whether the star is located in the star formation region. From Figure 8, we can tell that almost all of these candidates have distances within 200pc. The distance is so close that most of them are located in the front of star formation region. By comparing with the distance of several nearby star formation regions and molecular clouds (Bertout et al. 1999), like Taurus (Kenyon et al. 1994) and Ophiuchus (Knude & Hog 1998; Mamajek 2008), we found that none of our candidates were located in these nearby star formation regions or molecular clouds. They may just affect these sources as background. Kennedy & Wyatt (2012) shown that the *IRAS* 100 μ m background level should be lower than 5MJysr⁻¹. Of the 378 candidates left in Sec 2.4.2, 141 remain after this cut. One thing should be noted, all the 141 sources (red dots in Figure 1) locate in high latitude ($|l| > 10^\circ$). That is to say, the star formation regions affect slightly.

Figure 1 shows the Aitoff projection in the galactic coordinate. The molecular cloud and interstellar medium are located in the region between two black solid lines (Dame et al. 2001). For simplicity, those located in the high latitude are not plotted, which don't have big impact on our results. From Figure 1, we found that hardly any of these stars locates in the galactic disk because of high IR background.

2.5. Optical Observations

Using the selected sources from the observations of *Hipparcos* as described in section 2.4, we can obtain the Hertzsprung-Russell Diagram (HRD). From these candidates, we choose 6 stars ((red asterisk in Figure 9)) using for spectral observation and they all located in the main sequence of HRD. The detailed informations of observation are described bellow.

The optical spectra were obtained with NAOC's 2.16-m telescope at Xinglong, Beijing in Jan. 2012. The attached spectrograph is obtained with the grism G7 of BFOSC (Beijing Faint Object Spectrograph and Camera), and the spectrograph covers the wavelength range from $3870\text{\AA} \sim 6760\text{\AA}$. The exposure times were short because they are all bright stars. The detail informations of the spectral observations are listed in Table 1.

All these spectral data were reduced by the standard procedures with IRAF packages, which include overscan correction for BFOSC only, bias subtraction, flat-field correction. The Fe/Ar lamps were used for the wavelength calibration of BFOSC spectra. The standard stars used for the flux calibration at each night are Feige25, HZ14, EG247, GD71, respectively. All resulting spectra are shown in Figure 10. The spectral classifications are also given in Table 1, which is consistent with the spectral type given by *Hipparcos* Main catalog. The six stars are all the main-sequence dwarf stars with the spectral types from B8 to F0.

3. RESULTS AND DISCUSSION

3.1. Notes on Catalog

Then we present a catalog for our selected IR excess candidates, which containing the information provided in the *WISE* and *Hipparcos* Main Catalog. This catalog contains 38 known IR excess stars or debris disk candidates, 23 double or multiple stars, 12 variable stars and 4 Be stars. While the remaining more than 70 stars are identified as the $22\ \mu\text{m}$ excess candidates in our work.

3.1.1. Catalog of IR Excess Stars

The parameters of the catalog are list bellow: The *Hipparcos* name, *Hipparcos* RA and DEC (in the units of degree, J2000), spectral type (given by *Hipparcos*), the luminosity ratio (calculated in Section 3.4), photometric magnitude at optical *B*, *V* and *I* bands, *J*, *H*, *K_s* of 2MASS and four band of *WISE* and $K_s - [22]$ (mag, used as criterion for searching IR excess). The photometric magnitude uncertainty of each band is also listed. The Vega magnitude system has been used. The stars, which could be contaminated by the nearby stars that can not be excluded using likelihood-ratio method, are checked by optical images and marked in the last column.

The whole catalog has 141 IR excess candidates and each contains 18 columns. A summary of the column information is given in Table 2. They are presented in Table 3 for different types of stars.

3.1.2. Classification of IR excess stars

In the filtered catalog described in Section 3.1.1, 141 sources are included. All these stars show the IR excess feature at $22 \mu\text{m}$. To study the principle of showing IR excess, we checked all these sources and classified them into the following two types.

- Main-Sequence stars

As shown in Figure 9, some of them located in the giant stars region and most located in the main-sequence region. So we can separate the giant stars from the main-sequence stars in our catalog. The constraint $M_v > 6.0(B - V) - 2.0$ (dashed line in Figure 9) are used to separate main-sequence stars (blue plus symbol in Figure 9) from this sample (Rhee et al. 2007). The separation between main-sequence stars and giants can help us to understand the possible different mechanism of the IR excess stars. There are 140 main-sequence stars which are presented in Table 3. All these main-sequence stars cover spectral type range from B5 to K0 (Figure 11), and most have luminosity type IV and V. From the HRD (Figure 11), we can see that almost all our candidates belong to the main-sequence stars except one, so in order to avoid confusion, We remove the luminosity type from *Hipparcos* Main Catalog.

- Giants

As described above, there are only one giant (red plus symbol in Figure 9) which are listed in Table 3. Its spectral type is G5.

3.1.3. Contaminated Stars

In Section 3.1.2, we have classified them as main-sequence stars and giants. Though most of our candidates don't locate in the galactic disc and have no background effect, the IR excess may still be contributed from the companion star. So they are all noted in Table 3. We do this only by eyes. We plot the whole sample, as shown in Appendix A. From the optical and *WISE* 22 μm images, almost all these contaminated stars have companion objects around. Because we can not confirm that whether these stars are affected by the surroundings, so they are marked and can be used for further study.

There are 11 contaminated stars found in our candidates. The contaminated stars can not be excluded perfectly by using the likelihood ratio method, because many surroundings of the contaminated stars are fainter than the center sources. That is why we must check them from optical and mid-IR images.

3.2. The Coincidence Probability

Though we excluded the sources with the fuzzy features by using sources identification method (Section 2.4.2), it is still possible that some background and distant galaxies coincide with the position of our the candidates and contaminate the most radiation at 22 μm . Therefore, we need to estimate the coincidence probability for each source. According to Stauffer et al. (2005), we first obtained the cumulative sources counts for those with 22 μm magnitude brighter than the star itself. In fact, there is no need to calculate all candidates' coincidence probabilities. We just want to give the probability range. So we can roughly estimate the coincidence probability like this: Firstly, we assume the *WISE* all-sky data is evenly distributed. Then we select the faintest stars (6.775 mag at 22 μm band with $S/N \geq 20$) from the 141 candidates and estimate the cumulative sources counts with 22 μm magnitude less than 6.775 in *WISE* All-sky data catalog. The total number is about 2.5×10^6 , which means about 7.6×10^4 per steradian. It corresponds to about one source per 5.6×10^5 arcsec². Considering the previous matched radius of 6 arcsec. So this coincidence probability of background 22 μm source with magnitude less than 6.775 being close to the line of sight to the faintest candidates is about 0.0002. Moreover, from Figure 12 we can see that almost all the center coordinate errors are ≤ 3 arcsec. So we select 3 arcsec as the radius to calculate the coincidence probability. Then each coincidence probability of the 141 candidates is $\leq 5.0 \times 10^{-5}$. That is to say, within 3 arcsec radius, the probabilities of meeting another source is only 0.00005. In Section 2.2, there are about 100,000 *Hipparcos* sources used for matching with *WISE* catalog. We assume that the stars are evenly distributed, so the coincidence sources are ~ 5 . In fact, some of the coincidence sources can be excluded

with likelihood ratio method (Section 2.4.2). The coincidence probability is so small that the star is almost impossible to be contaminated which locates in the low-density star region (like the high galactic latitude region). However, for those locate in the high density region, we still can not exclude the possible contamination by interstellar medium or background AGN (Stauffer et al. 2005). So we should check the contaminated sources from the optical images (Section 3.1.3).

3.3. Color-Color Diagram

Figure 2 shows the $J - H$ versus $K_s - [22]$ diagram for all matched stars from *WISE* and *Hipparcos* Main catalog. The gray dots are those have no excess at $22\mu\text{m}$ band and the black solid curve shows the normal dwarf stars labeled with corresponding spectral types. Main-sequence stars and Giants with IR excess are plotted as blue, red plus symbol respectively. Red dotted line is the selection criterion from Section 2.4. From Figure 2, most of stars locate nearby the criterion line. The only one giant star locates $J - H > 0.5$ in our sample. Most are excluded because of high $100\ \mu\text{m}$ background level.

Figure 13 shows the $J - H$ vs $K - [12]$ color-color diagram for the stars showing IR excess at $22\ \mu\text{m}$ band. The blue plus signs represent the main-sequence stars and red plus signs for Giants. So as to be convenient for comparing, the x, y zero axes (gray dotted line) and all matched (*WISE* and *Hipparcos*) sources are plotted (gray plus signs). As shown in this figure, many main-sequence stars trend to have $K - [12] = 0$. While the only one giant star trend to have excesses at $12\ \mu\text{m}$ band. That is to say, comparing with the main-sequence stars, giants have larger luminosity at $12\ \mu\text{m}$ band, and this implies that the dust around giants is hotter.

The $W3 - W4$ vs $J - H$ color-color diagram is shown in Figure 14. From Figure 14 we can see that very few stars locate nearby the Y axis. Those with $W3 - W4 \leq 0.1$ (left of or nearby the Y axis) are HIP 70386, HIP 22531, HIP 67953, HIP 30174, HIP 42753, HIP 12351, HIP 72138 and HIP 29888. Of the 8 sources, they are all double or multiple stars except HIP 12531. That is to say, if the excess at $22\ \mu\text{m}$ band is from the binary or the companion which can not be resolved by WISE, then $W3 - W4$ should trend to be zero. While the trend can not be seen from Figure 14. So we can conclude that the excess in most of our candidates is not from the binary or companion. The known binary and multiple systems have been noted in Table 3.

We have described in Section 2.1, there is an overestimate at $4.6\ \mu\text{m}$ band for brightness stars. We also found the effect in this work. When we plot the $[3.4] - [4.6]$ vs $[3.4] - [12]$ (or

[3.4] – [22]) diagram, we find that almost all of the giants and 1/4 of main-sequence stars located at [3.4] – [4.6] = 0.5 while most located at [3.4] – [12] = 0, that is unreasonable! The phenomenon is similar to the bias mentioned in Tisserand (2012) and the bias found in this paper is about 0.5 mag. WISE team also reported this effect but gave no explain.

3.4. The Dust Fraction

In order to characterize the amount of dust, the ratio of integrated infrared excess luminosity to bolometric one of a star, $f_d = L_{\text{IR}}/L_* = F_{\text{IR}}/F_*$ (Moór et al. 2006; Carpenter et al. 2009) is introduced. In this section, we will introduce two method to estimate the dust fraction f_d for all the candidates.

First, because we don't have far-infrared fluxes for all these stars because of no longer bands in *WISE*. So we assumed νL_ν as the total infrared luminosity L_{IR} (Chen et al. 2005a; Wu et al. 2012). Considering the bolometric luminosities of stars, we integrated the whole flux with different band. Then the dust fraction for each candidate can be estimated which is listed in Table 3.

The second method is from Beichman et al. (2005).

$$\frac{L_{dust}}{L_*}(\text{minimum}) = 10^{-5} \left(\frac{5600K}{T_*} \right)^3 \frac{F_{70,dust}}{F_{70,*}} \quad (7)$$

The fractional luminosity derived by Beichman et al. (2005) depends on the dust temperature. We set the emission peak at 22 μm , which means $T_{dust} \approx 150$ K. Then the minimum fractional luminosity can be calculated. The results from the two methods mainly range from 10^{-5} even to 10^{-3} . The histogram of dust fraction for all candidates is plotted in Figure 15.

Beichman et al. (2005) point that the fractional luminosity can be used as an age indicator. But there is no yet final conclusion. Zuckerman & Song (2004) hypothesised that stars with $f_d > 10^{-3}$ are younger than 100 Myr and Beichman et al. (2005) also suggested a decline in the fraction of stars with excess IR emission with time. On the contrary, Decin et al. (2003) claimed the existence of high f_d disks around older stars and they also found that the fractional luminosity show a large spread ($10^{-6} - 10^{-3}$) at almost any age. Although we don't know yet which point of the two is supported in this paper, we can obtain one another conclusion. Obviously it can be seen in Figure 15 that the giants have higher f_d than main-sequence stars. It can be explained as the stars at the late evolutionary stages have more luminosity at mid-infrared band, which is also consistent with the characteristics of giants.

If some older stars with higher f_d in our galaxy, they are really rare systems up to

date (Wu et al. 2012). Although Rieke et al. (2005) suggested that the dust would be more plentiful in the late stages of planet formation from planetesimals collisions and cometary activity, this can not fully explain the high fractional luminosity phenomena of the old stars. The most plausible explanation for the presence of debris disk with high fractional luminosity at ages well above Gyr is delay onset of collisional cascades by late planet formation further away from the star (Dominik & Decin 2003). However whether such a mechanism can also explain very old stars at ages of 10Gyrs is still questionable. The bottom line is to confirm the ages of these stars with the high fractional luminosity.

3.5. Images and Spectral Energy Distribution

We present all the optical images and SEDs for our sample. The figures are shown in appendix A. The images are from DSS (Digitized Sky Survey) and the positions are also marked on the optical images as red circle with a radius of $6''$. The SEDs cover all the wavelength range from the optical to the mid-IR bands, including the available photometry data from *Hipparcos* (B, V and I), 2MASS (J, H and K_s), and *WISE* (W3 and W4). All these SEDs are fitted by the blackbody formula. Our candidates is very bright, to avoid the influence of saturation, so the [3.4] and [4.6] band do not be used for SEDs fitting. The SEDs provided in this paper can be used to test our $K - [22]$ method of searching IR excess.

3.6. Candidates with Planets and Debris Disks Candidates

Bryden et al. (2009) have searched for debris disks and planets using *Spitzer's* MIPS far-IR camera, but did not find the correlation between planets and dust around. We cross-matched our catalog with known IR-excess Hipparcos stars hosting planets (Maldonado et al. 2012). It turns out that none was found. Similar with Kennedy & Wyatt (2012), those matched may all be excluded from our analysis because their higher background level or higher photometric error. We also cross-matched our catalog with *Kepler* planet candidates (Batalha et al. 2012), none was found. This is because our samples are brighter than the *Kepler* candidates. We still compared our candidates with debris disks candidates in Rhee et al. (2007), which studied the debris disks from the *IRAS* and *Hipparcos* catalog, and 27 sources are matched, they are all noted in the total catalog (Table 3). By comparing with previous conclusion, there are 38 known IR excess stars or debris disk candidates. They are all noted in Table 3. Those not be matched may contain the new debris disks candidates which can not be found by *IRAS*.

By doing this, we want to know that if we can confirm the existence of the extra-solar planet around an IR-excess star, we could attribute the IR excess to their asteroid belt. But we don't found known candidates with planets from the 141 IR excess stars. This can be explained by two points. One is that the excess of the 141 stars is from only dust, the other is that some unknown candidates with planets included have not been found.

3.7. Fraction of Main-Sequence Stars with IR Excess

In our sample, we count the number of stars with IR excess for main-sequence stars. Using the threshold mentioned in Section 2.2, the cross-matched catalog contains about 7,624 sources whose spectral types are either main-sequence or giants. Filtering the giant stars with $M_v > 6.0(B - V) - 2.0$ and dropping those with high IRAS 100 μm background level, we found about 2,649 main-sequence sources without background contamination, which yields the fraction of main-sequence stars, about $140/2649 \sim 5.30\%$, while the fraction of FGK main-sequence stars is $42/1897 \sim 2.21\%$. Noting that the number here is less than the $9\% \sim 17\%$ derived by Hovhannisyan et al. (2009), 10% concluded by Meyer et al. (2008). This is mainly because we set the definition of IR excess with 4σ . When 3σ is used, then the detection rate of FGK main-sequence is $130/1897 \sim 6.85\%$. Of which, 130 means the number of FGK main-sequence stars with $22 \mu\text{m}$ excess by using 3σ definition. In addition, there are other reasons. Because we focus only on the very bright all-sky stars and exclude the stars with higher IRAS 100 μm background. It means that almost all the stars locate in the galactic disk or star formation region are removed. According to the common sense, the IR excess stars locate in the low galactic latitude (like galactic disk or star formation region) are more than those locate in the high galactic latitude. Moreover, the originally selecting criterion of W4 $S/N \geq 20$ can lower the detection rate.

Figure 11 shows the distribution of main-sequence stars with IR excess, the Y axis is the detection rates of different spectral types. The corresponding error bars (1σ) are also drawn. The error bars are calculated by using the error of $K - [22]$, so the upper limit and the lower limit are not the same. Because K and M type stars with $22 \mu\text{m}$ excess are very few, we hardly see the error bar of K typr stars and the lower limit of M stars. From Figure 11 we can see that B, A and M type stars have more IR excess than others. More detailed numbers can be seen in Table 4.

4. SUMMARY

We present a catalog which includes 141 IR excess stars at $22\mu\text{m}$. All these stars are selected from *WISE* All-sky data cross-correlated with *Hipparcos* Main Catalog. By examining the WISE data for these selected candidates, we conclude that they all show an IR excess at $22\mu\text{m}$ (i.e., $K_s - [22] \geq 0.26$ for $J - H \leq 0.1$, $K_s - [22] \geq 0.21$ for $0.1 < J - H \leq 0.3$, $K_s - [22] \geq 0.22$ for $0.3 < J - H \leq 0.5$ and $K_s - [22] \geq 0.22$ for $J - H > 0.5$). With the help of *Hipparcos* Main Catalog, we can classify them as different type for detailed study according to IR excess production mechanism, and the corresponding catalogs are given in appendix. In this paper, we provide, for all the IR-excess candidates, the SEDs from optical to mid-infrared and optical images, and we also give the infrared dust fraction. Reading from the color-color diagram, we can tell that most main sequence stars show IR excess at only $22\mu\text{m}$ while giants at both $12\mu\text{m}$ and $22\mu\text{m}$.

Generally speaking, the IR excess stars could be used to search for exoplanets, so we cross-matched our catalog with known IR excess stars having planets and *Kepler* planet candidates, but none is matched. They are all filtered out by our criterion, the explanations are also given.

Lastly, we count the number of stars showing IR excess for different spectral type of main-sequence stars and also give the explanations to them.

The IR excess star catalog in this work can be used as the input for many future study, e.g., searching extra-solar planets, searching stars with debris disk and modeling the surrounding disk, studying the mechanism of showing IR excess.

5. Acknowledgements

Ch-J, Wu thanks Li-Jun Gou, Lian Yang and Jun-Li Cao for warmhearted help and Xu Zhou for valuable discussion. we sincerely thank the anonymous referee whose suggestions greatly helped us improve this paper. This project is supported by the China Ministry of Science and Technology under the State Key Development Program for Basic Research (2014CB845705, 2012CB821800), the National Natural Science Foundation of China (Grant Nos. 11173030, 11225316, 11078017, 10833006, 10978014 and 10773014), the Key Laboratory of Optical Astronomy, the National Astronomical Observatories, Chinese Academy of Sciences, the National Science Foundation of China (Grants No. 11173006), the Ministry of Science and Technology National Basic Science program (project 973) under grant No. 2012CB821804, and the Fundamental Research Funds for the Central Universities.

This publication makes use of data products from the Wide-field Infrared Survey Explorer, which is a joint project of the University of California, Los Angeles, and the Jet Propulsion Laboratory/California Institute of Technology, funded by the National Aeronautics and Space Administration.

In this work, we made extensive use of the Hipparcos Catalogs (ESA 1997), which is the primary result of the Hipparcos space astrometry mission, undertaken by the European Space Agency, with the scientific aspects undertaken by nearly two hundred scientists within the NDAC, FAST, TDAC and INCA Consortia.

Facilities: 2.16m Telescope (NAOC), WISE, HIPPARCOS

REFERENCES

- Aumann, H. H., Beichman, C. A., Gillett, F. C., et al. 1984, *ApJ*, 278, L23
- Avenhaus, H., Schmid, H. M., & Meyer, M. R. 2012, *A&A*, 548, A105
- Batalha, N. M., Rowe, J. F., Bryson, S. T., et al. 2012, *ArXiv e-prints*: 1202.5852
- Beichman, C. A., Bryden, G., Rieke, G. H., et al. 2005, *ApJ*, 622, 1160
- Bertout, C., Robichon, N., & Arenou, F. 1999, *A&A*, 352, 574
- Bryden, G., Beichman, C. A., Carpenter, J. M., et al. 2009, *ApJ*, 705, 1226
- Carpenter, J. M., Bouwman, J., Mamajek, E. E., Meyer, M. R., Hillenbrand, L. A., Backman, D. E., Henning, T., Hines, D. C., Hollenbach, D., Kim, J. S., Moro-Martin, A., Pascucci, I., Silverstone, M. D., Stauffer, J. R., & Wolf, S. 2009, *ApJS*, 181, 197
- Chen, C. H., Jura, M., Gordon, K. D., & Blaylock, M. 2005a, *ApJ*, 623, 493
- Chen, C. H., Patten, B. M., Werner, M. W., et al. 2005b, *ApJ*, 634, 1372
- Ciliegi, P., Zamorani, G., Hasinger, G., et al. 2003, *A&A*, 398, 901
- Dame, T. M., Hartmann, D., & Thaddeus, P. 2001, *ApJ*, 547, 792
- Debes, J. H., Hoard, D. W., Wachter, S., et al. 2011, *ApJS*, 197, 38
- Decin, G., Dominik, C., Waters, L. B. F. M., & Waelkens, C. 2003, *ApJ*, 598, 636
- Dominik, C. & Decin, G. 2003, *ApJ*, 598, 626

- Gáspár, A., Rieke, G. H., & Balog, Z. 2013, *ApJ*, 768, 25
- Gorlova, N., Padgett, D. L., Rieke, G. H., et al. 2004, *ApJS*, 154, 448
- Gorlova, N., Rieke, G. H., Muzerolle, J., et al. 2006, *ApJ*, 649, 1028
- Hoard, D. W., Wachter, S., Sturch, L. K., et al. 2007, *AJ*, 134, 26
- Hovhannisyan, L. R., Mickaelian, A. M., Weedman, D. W., et al. 2009, *AJ*, 138, 251
- Iverson, R. J., Greve, T. R., Dunlop, J. S., et al. 2007, *MNRAS*, 380, 199
- Kennedy, G. M. & Wyatt, M. C. 2012, *MNRAS*, 426, 91
- Kenyon, S. J., Dobrzycka, D., & Hartmann, L. 1994, *AJ*, 108, 1872
- Kim, J. S., Hines, D. C., Backman, D. E., et al. 2005, *ApJ*, 632, 659
- Knude, J. & Hog, E. 1998, *A&A*, 338, 897
- Koerner, D. W., Kim, S., Trilling, D. E., et al. 2010, *ApJ*, 710, L26
- Lagrange, A.-M., Backman, D. E., & Artymowicz, P. 2000, *Protostars and Planets IV*, 639
- Lawler, S. M. & Gladman, B. 2012, *ApJ*, 752, 53
- Low, F. J., Smith, P. S., Werner, M., et al. 2005, *ApJ*, 631, 1170
- Mainieri, V., Kellermann, K. I., Fomalont, E. B., et al. 2008, *ApJS*, 179, 95
- Maldonado, J., Eiroa, C., Villaver, E., et al. 2012, *A&A*, 541, A40
- Mamajek, E. E. 2008, *Astronomische Nachrichten*, 329, 10
- Meyer, M. R., Carpenter, J. M., Mamajek, E. E., et al. 2008, *ApJ*, 673, L181
- Meyer, M. R., Hillenbrand, L. A., Backman, D. E., et al. 2004, *ApJS*, 154, 422
- Mizusawa, T. F., Rebull, L. M., Stauffer, J. R., Bryden, G., Meyer, M., & Song, I. 2012, *AJ*, 144, 135
- Moór, A., Abraham, P., Derekas, A., et al. 2006, *ApJ*, 644, 525
- Morales, F. Y., Padgett, D. L., Bryden, G., Werner, M. W., & Furlan, E. 2012, *ApJ*, 757, 7

- Morales, F. Y., Werner, M. W., Bryden, G., Plavchan, P., Stapelfeldt, K. R., Rieke, G. H., Su, K. Y. L., Beichman, C. A., Chen, C. H., Grogan, K., Kenyon, S. J., Moro-Martin, A., & Wolf, S. 2009, *ApJ*, 699, 1067
- Perryman, M. A. C., Lindegren, L., Kovalevsky, J., et al. 1995, *A&A*, 304, 69
- . 1997, *A&A*, 323, L49
- Rebull, L. M., Stapelfeldt, K. R., Werner, M. W., Mannings, V. G., Chen, C., Stauffer, J. R., Smith, P. S., Song, I., Hines, D., & Low, F. J. 2008, *ApJ*, 681, 1484
- Rhee, J. H., Song, I., Zuckerman, B., & McElwain, M. 2007, *ApJ*, 660, 1556
- Ribas, Á., Merín, B., Ardila, D. R., & Bouy, H. 2012, *A&A*, 541, A38
- Richter, G. A. 1975, *Astronomische Nachrichten*, 296, 65
- Rieke, G. H., Su, K. Y. L., Stansberry, J. A., et al. 2005, *ApJ*, 620, 1010
- Rieke, G. H., Young, E. T., Engelbracht, C. W., et al. 2004, *ApJS*, 154, 25
- Smith, D. J. B., Dunne, L., Maddox, S. J., et al. 2011, *MNRAS*, 416, 857
- Stauffer, J. R., Rebull, L. M., Carpenter, J., et al. 2005, *AJ*, 130, 1834
- Su, K. Y. L., Rieke, G. H., Stansberry, J. A., et al. 2006, *ApJ*, 653, 675
- Sutherland, W. & Saunders, W. 1992, *MNRAS*, 259, 413
- Thompson, R. I. 1982, *ApJ*, 257, 171
- Tisserand, P. 2012, *A&A*, 539, A51
- Touhami, Y., Gies, D. R., & Schaefer, G. H. 2011, *ApJ*, 729, 17
- Wachter, S., Hoard, D. W., Hansen, K. H., et al. 2003, *ApJ*, 586, 1356
- Wellhouse, J. W., Hoard, D. W., Howell, S. B., et al. 2005, *PASP*, 117, 1378
- Werner, M. W., Uchida, K. I., Sellgren, K., et al. 2004, *ApJS*, 154, 309
- Wright, E. L., Eisenhardt, P. R. M., Mainzer, A. K., et al. 2010, *AJ*, 140, 1868
- Wu, H., Wu, C.-J., Cao, C., et al. 2012, *RAA*, 12, 513
- Young, E. T., Lada, C. J., Teixeira, P., et al. 2004, *ApJS*, 154, 428

Zuckerman, B. 2001, *ARA&A*, 39, 549

Zuckerman, B., Rhee, J. H., Song, I., & Bessell, M. S. 2011, *ApJ*, 732, 61

Zuckerman, B. & Song, I. 2004, *ARA&A*, 42, 685

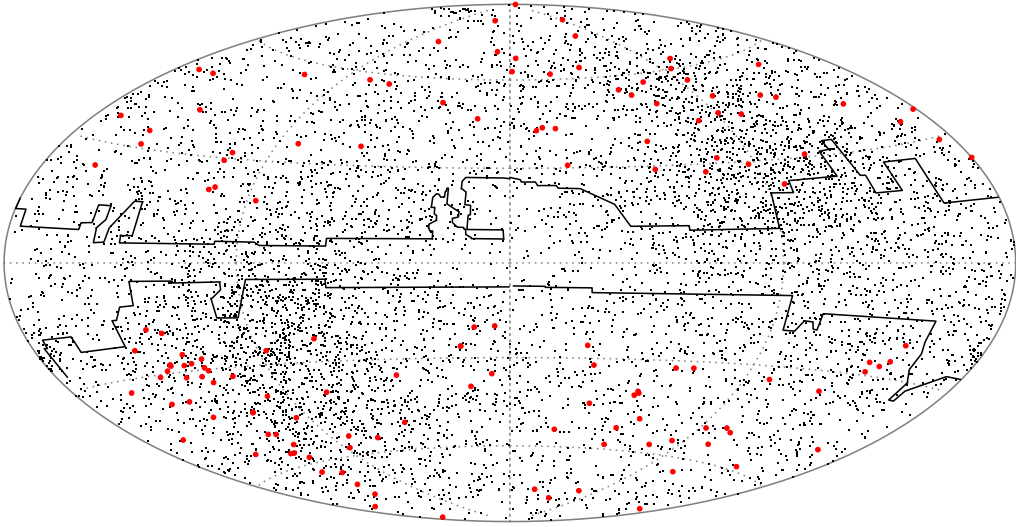


Fig. 1.— Distribution of IR excess stars. We show the distribution of matched catalog from *WISE* All-Sky Catalog and *Hipparcos* Main catalog in this figure (Gray dots); and the red points are the 141 IR excess candidates selected in this work. The region between black solid line is the star formation region. They all show in a galactic Aitoff projection.

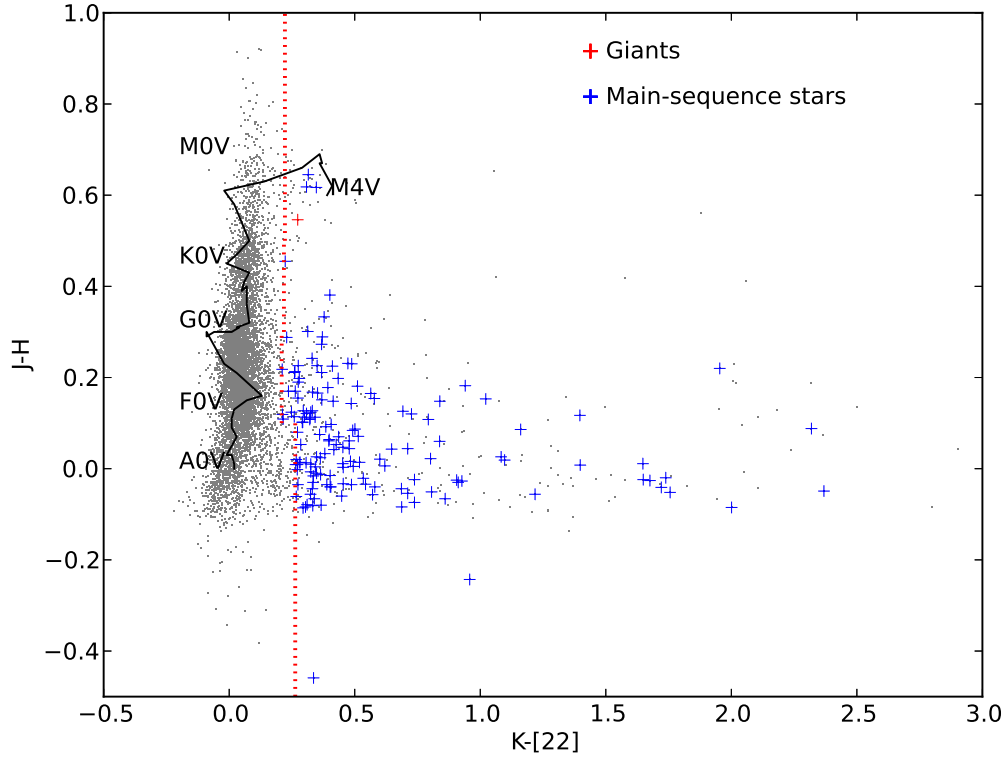


Fig. 2.— Diagram of $J-H$ vs $K_s-[22]$. The distribution of main-sequence stars and Giants are plotted as blue and red plus symbol respectively. The black solid line shows the normal dwarf stars labeled with the corresponding spectral types. The red dotted line gives our criterion for selecting the $22\ \mu\text{m}$ excess sources.

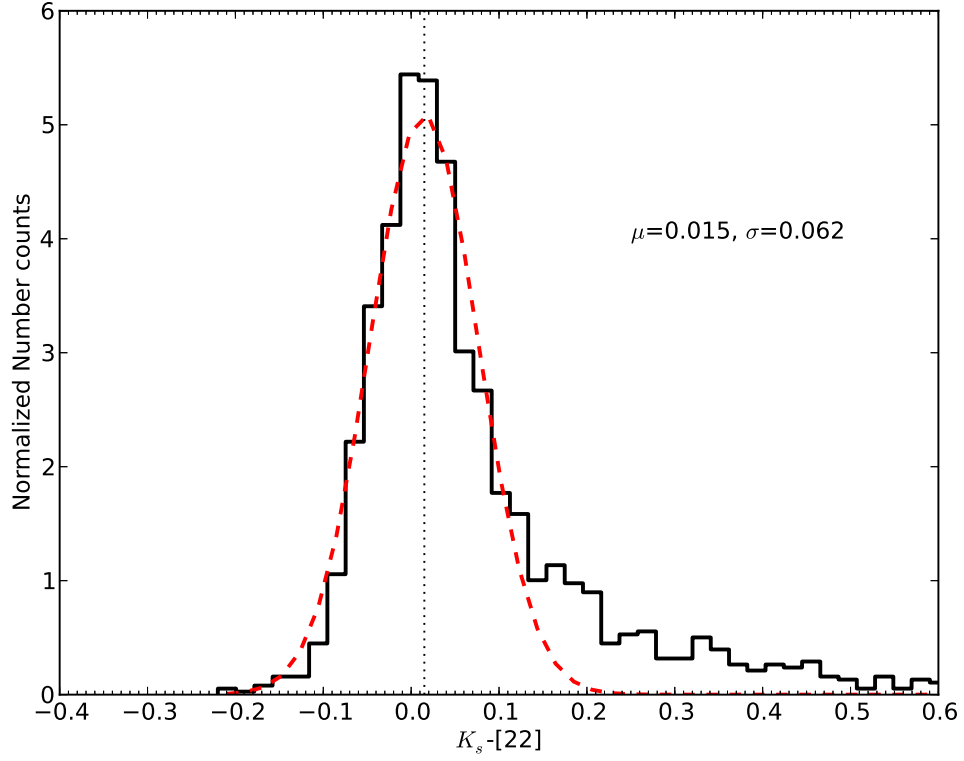


Fig. 3.— Goodness of fit for sources with $J - H \leq 0.1$. The criterion is $K_s - [22]_{\mu m} \geq 0.26$.

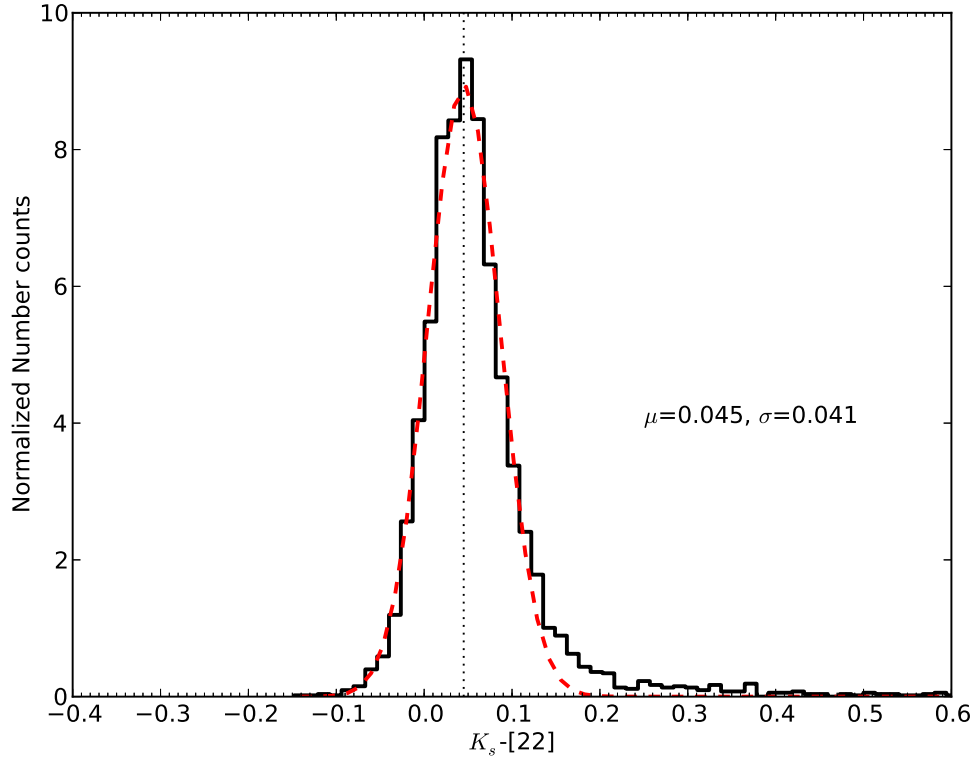


Fig. 4.— Goodness of fit for sources with $0.1 < J - H \leq 0.3$. The criterion is $K_s - [22]_{\mu m} \geq 0.21$.

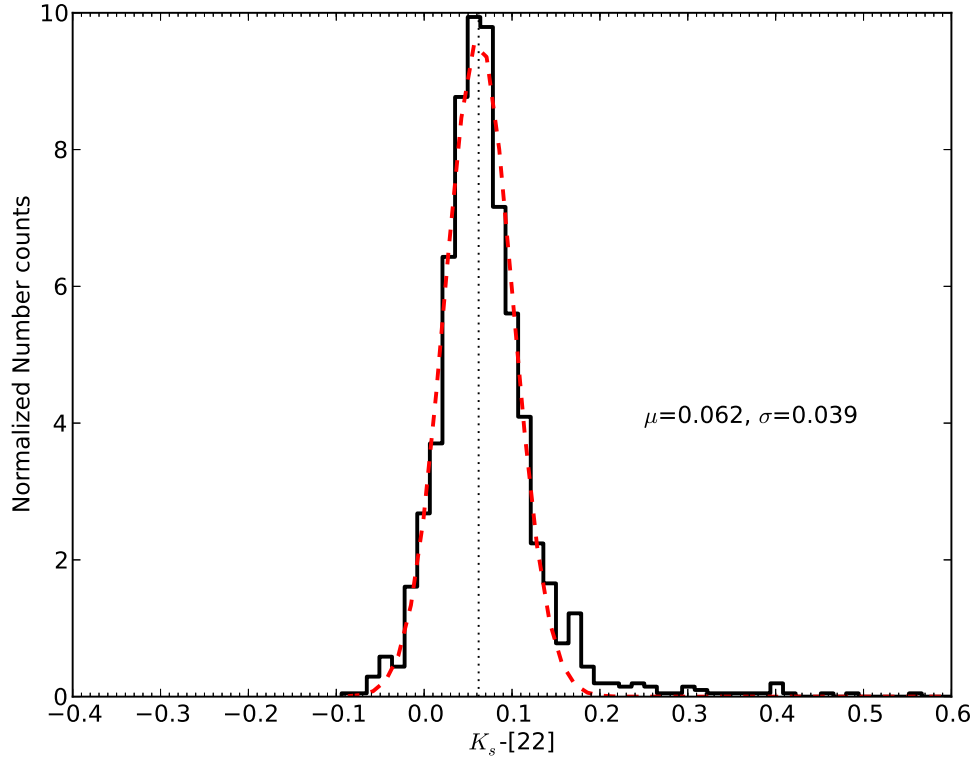


Fig. 5.— Goodness of fit for sources with $0.3 < J - H \leq 0.5$. The criterion is $K_s - [22]_{\mu m} \geq 0.22$.

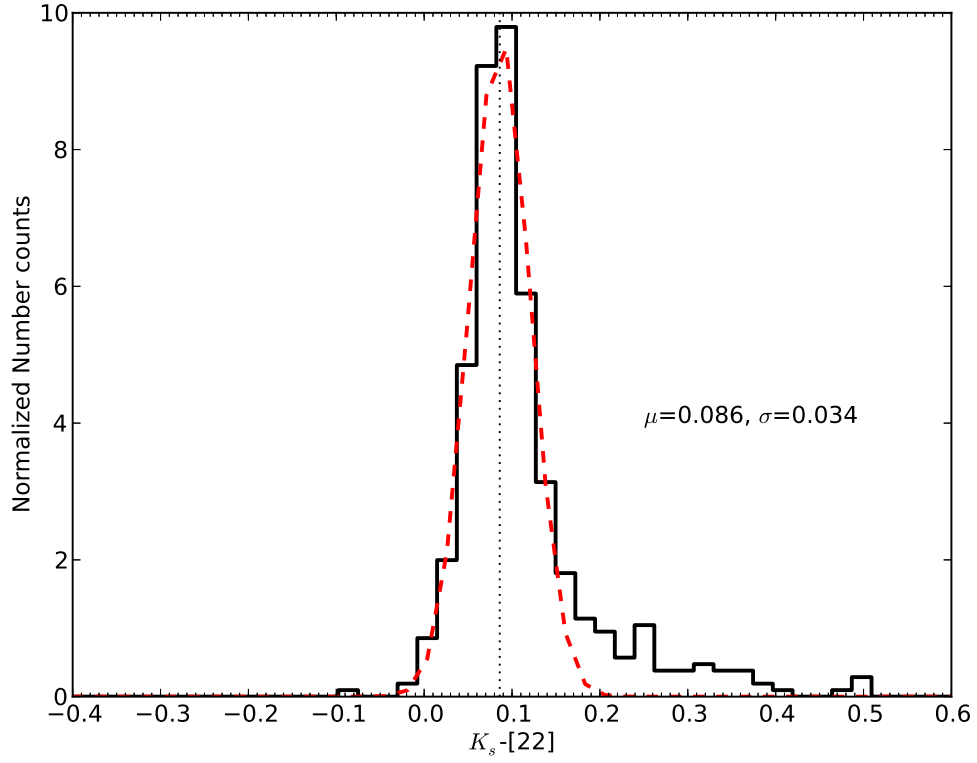


Fig. 6.— Goodness of fit for sources with $J - H > 0.5$. The criterion is $K_s - [22]_{\mu m} \geq 0.22$

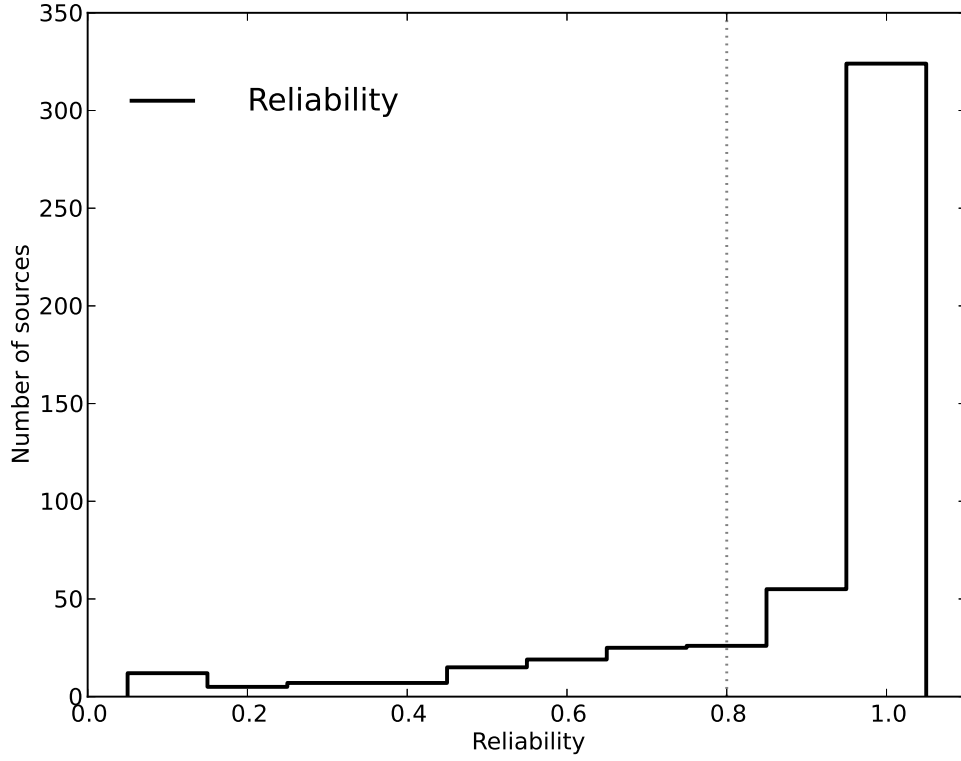


Fig. 7.— Reliability histogram of all the candidates. The dotted line shows the selection threshold. Those with reliability $R < 0.8$ are excluded.

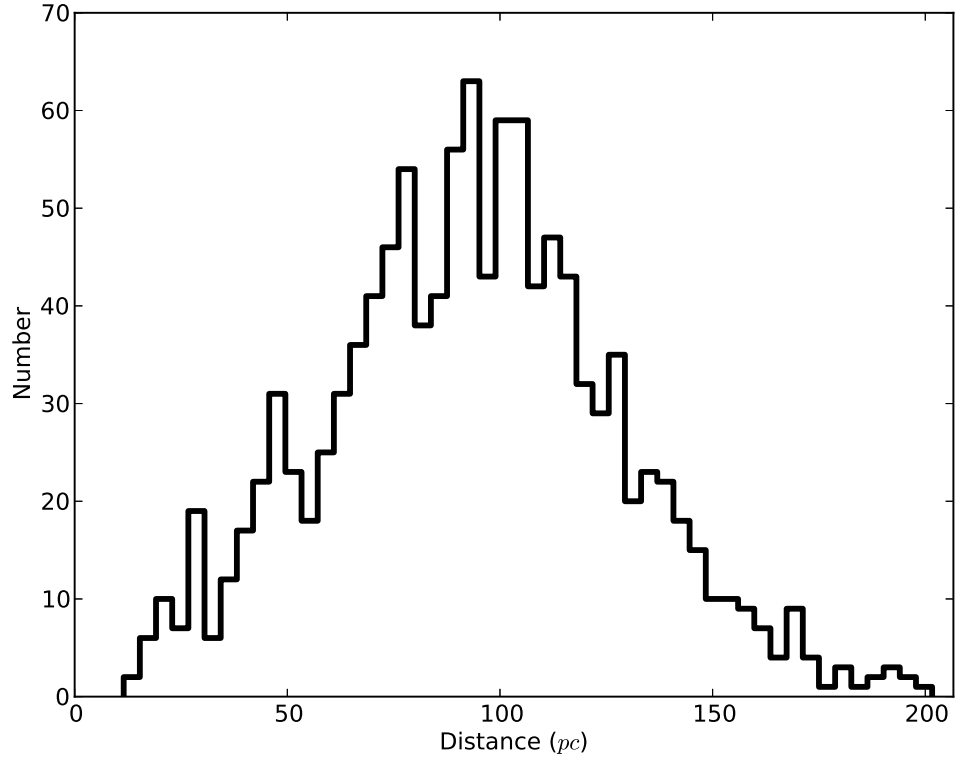


Fig. 8.— Distance distributions of all the candidates. The distance ranges within 200 pc. The distance is so close that most of them locate in front of star formation region.

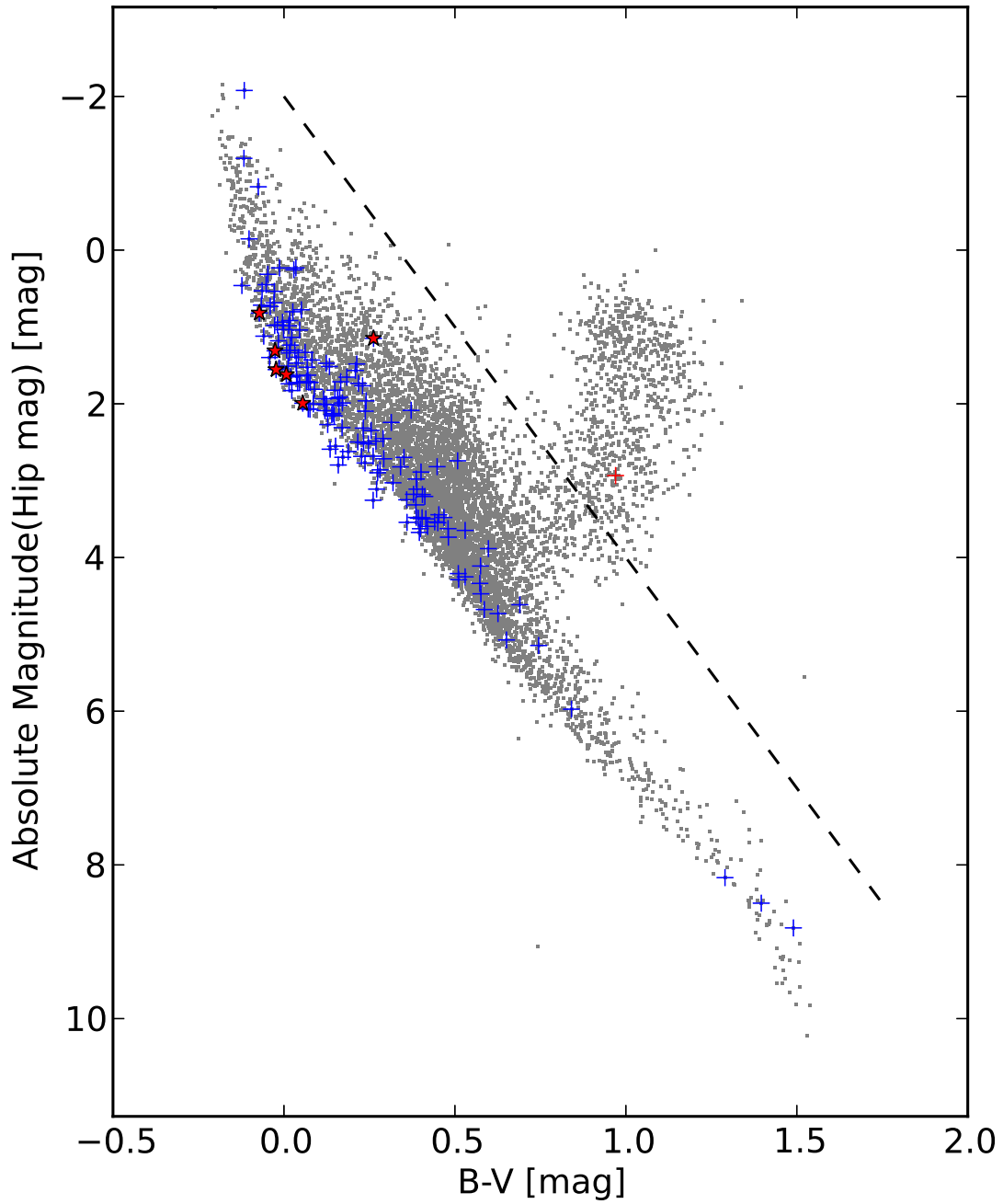


Fig. 9.— HRD of matched sources, main-sequence stars and giant stars. As shown in this figure, gray is the matched Hippocampus main catalog with WISE, blue represents the main-sequence stars with IR excess and red represents the giants. The 6 red asterisks are observed by 2.16m Telescope. Main-sequence stars and giants are separated by the criterion $M_v > 6.0(B - V) - 2.0$ (indicated with dashed line).

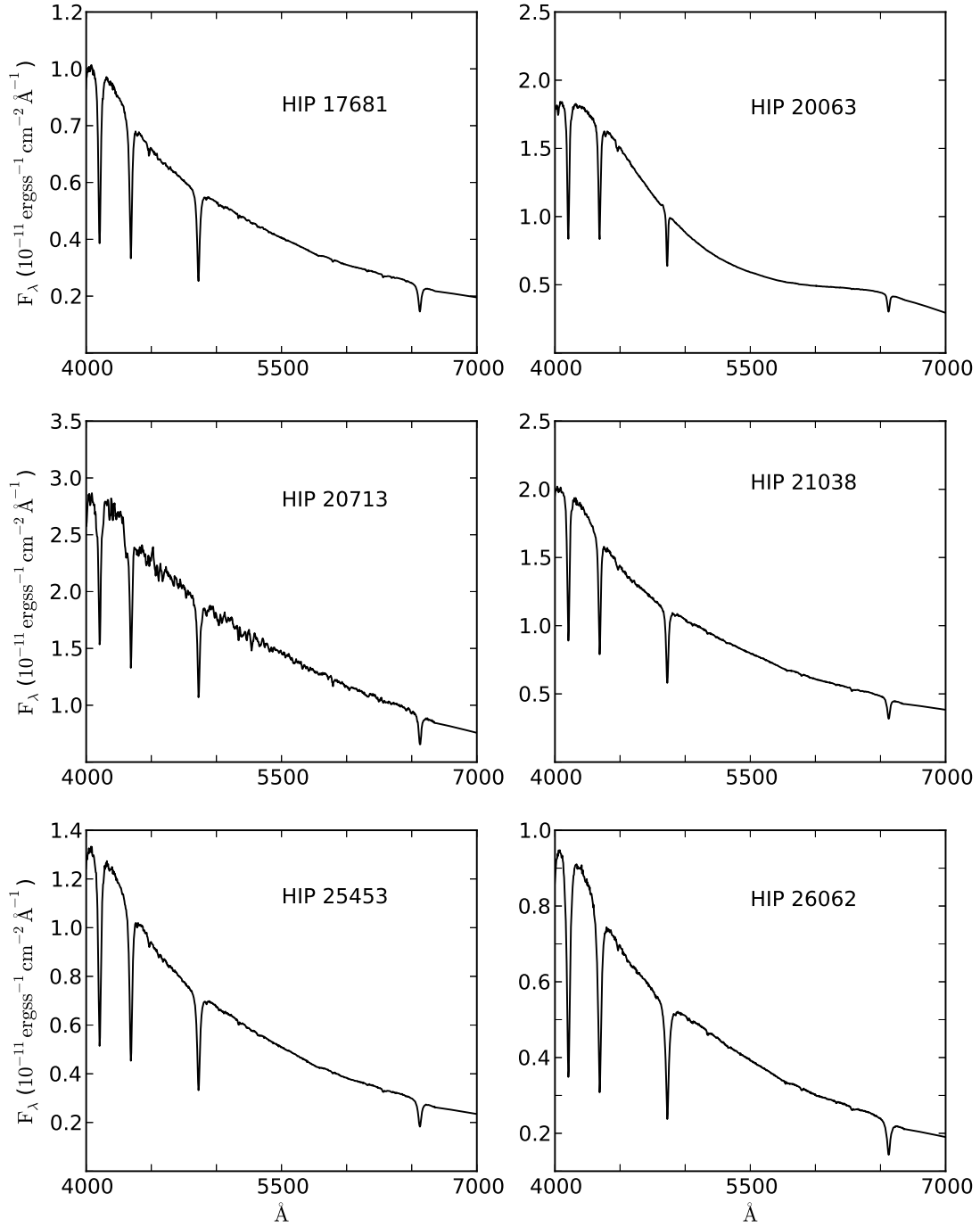


Fig. 10.— The observed optical spectra of six 22 μm excess stars. All stars have high S/N and present the main-sequence star features, covering the spectral types from B8 to F0.

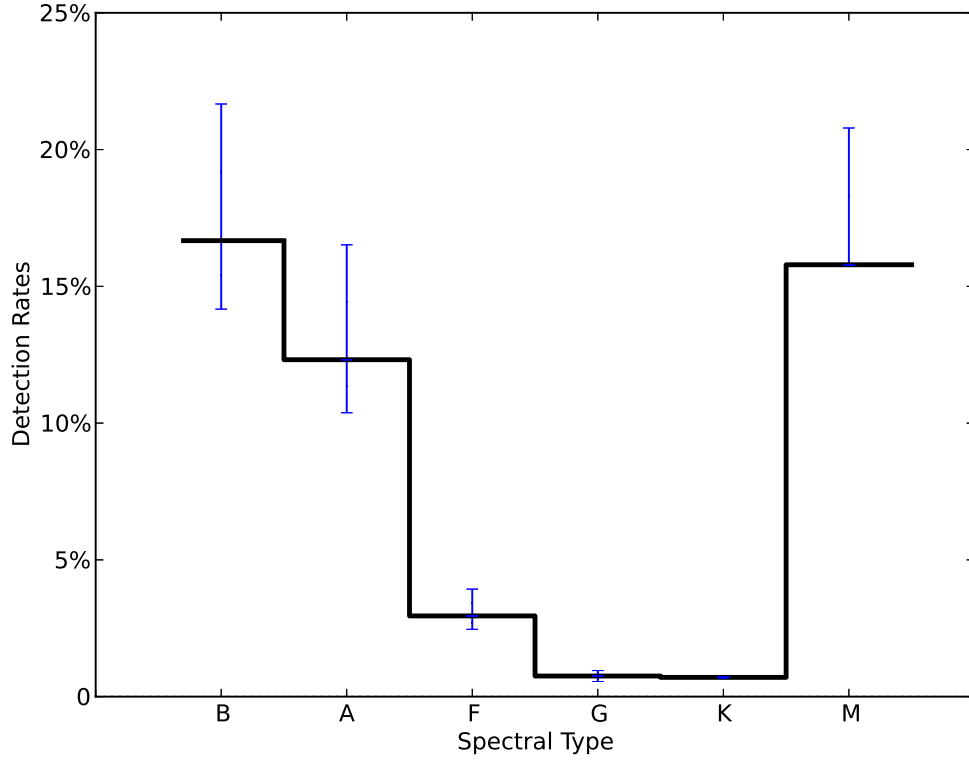


Fig. 11.— Detection rates of different spectral type stars showing IR excess, the corresponding error bars (1σ) are also shown.

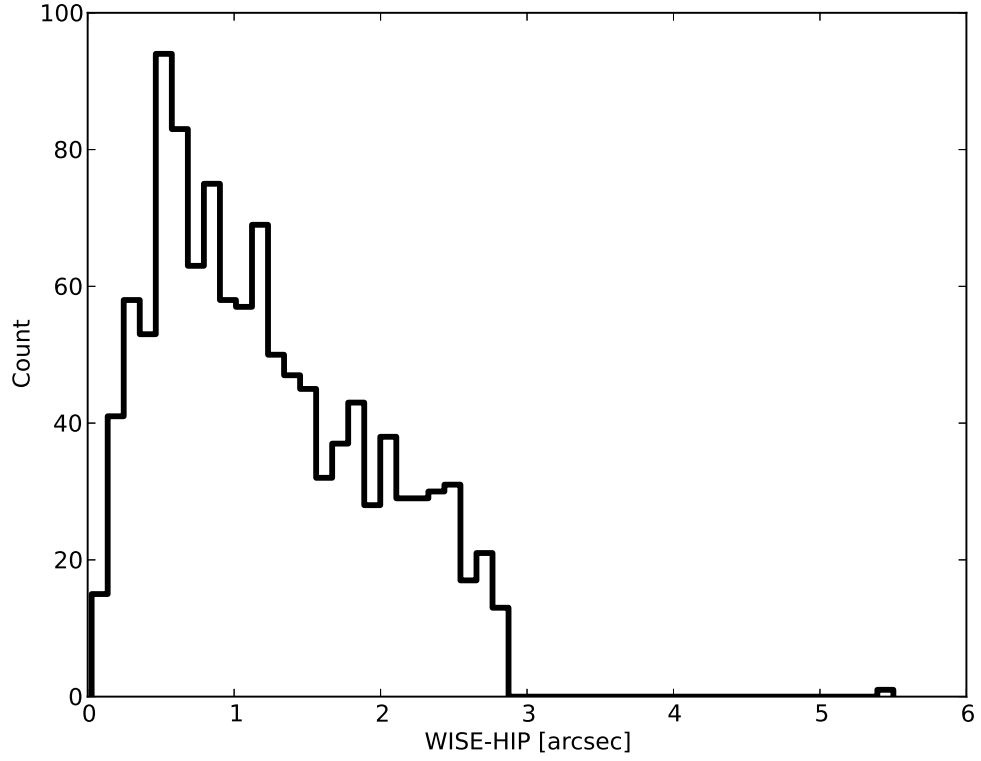


Fig. 12.— Center offset histogram of all the candidates between optical band and IR band. As shown in this figure, most stars except one have an uncertainty ≤ 3 arcsec. Thus we use 3 arcsec as the radius for calculating the coincidence probability.

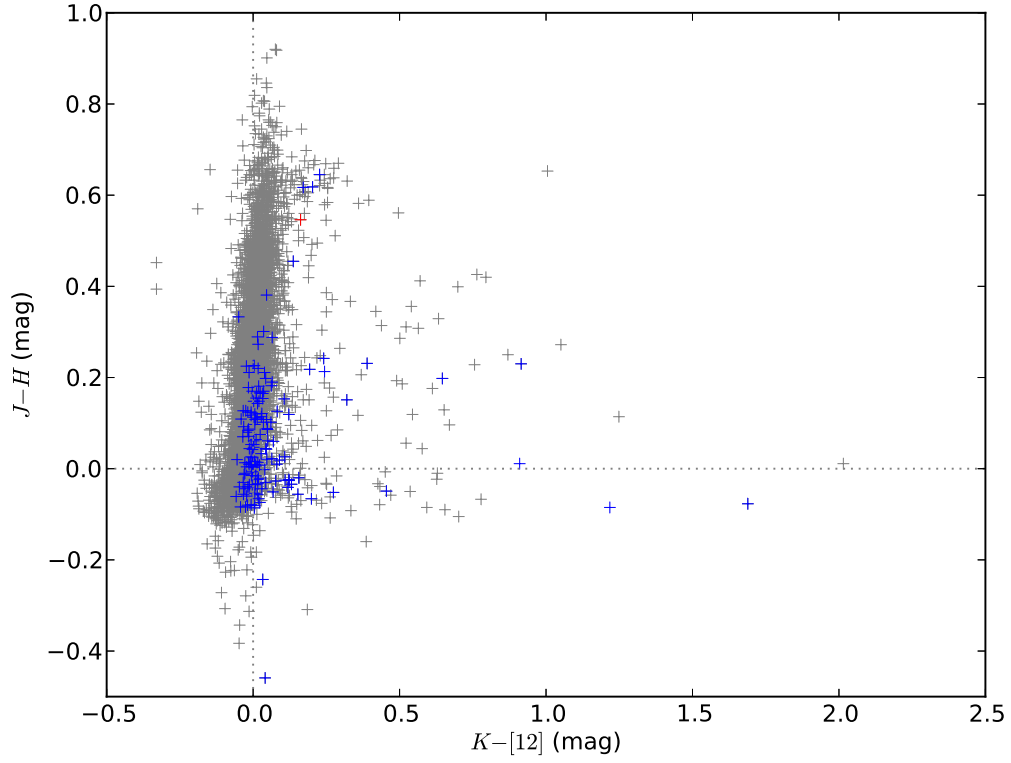


Fig. 13.— $K-[12]$ vs $J-H$ color-color diagram of $22\ \mu\text{m}$ excess stars. Blue plus symbols and red plus symbols represent main-sequence stars and giants respectively. Gray plus symbols mean all the matched sources from *WISE* and *Hipparcos*.

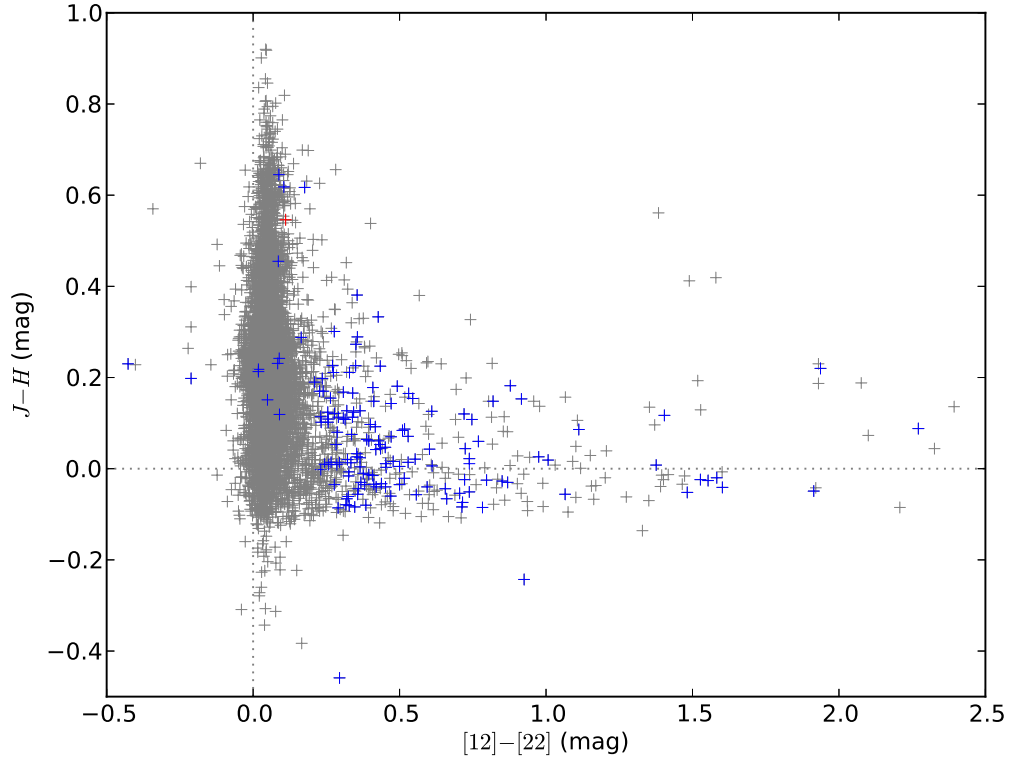


Fig. 14.— $W3 - W4$ vs $J - H$ color-color diagram of $22 \mu\text{m}$ excess stars. Blue plus symbols and red plus symbols represent main-sequence stars and giants respectively. Gray plus symbols mean all the matched sources from *WISE* and *Hipparcos*. Only a few stars locate nearby the Y axis.

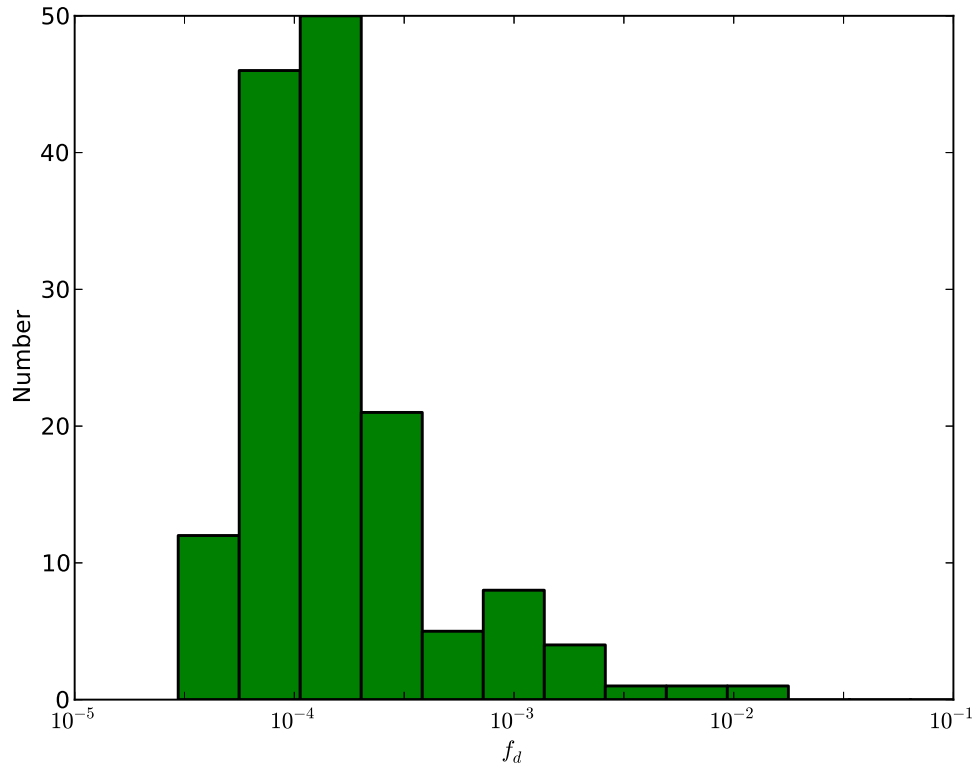


Fig. 15.— Histogram for the fractional luminosity f_d .

Table 1. Log of observation and spectral type for 6 selected stars showing excess at $22 \mu\text{m}$ band

Name	RA (J2000)	DEC (J2000)	Instrument	Slit (arcsec)	Plx (mas)	SpType (2.16m Telescope)	SpType (<i>Hipparcos</i>)	Date of Obs.
HIP 17681	03 47 16.10	+44 04 25.7	BFOSC Grism#7	1.8	8.13	B9	B9	(01.21.2012)
HIP 20063	04 18 08.09	+42 08 28.5	BFOSC Grism#7	1.8	8.39	B9	B9V	(01.21.2012)
HIP 20713	04 26 20.67	+15 37 06.0	BFOSC Grism#7	1.8	20.86	F0	F0V...	(01.21.2012)
HIP 21038	04 30 38.40	+32 27 28.1	BFOSC Grism#7	1.8	10.63	B9	B9.5Vn	(01.21.2012)
HIP 25453	05 26 38.82	+06 52 07.5	BFOSC Grism#7	1.8	10.68	A0	A0Vn	(01.21.2012)
HIP 26062	05 33 30.75	+24 37 44.1	BFOSC Grism#7	1.8	10.0	B8	B8	(01.21.2012)

Table 2. $22 \mu\text{m}$ Stars Excess Catalog Format

Column	Name	Units	Description
1	HIP	—	Name of stars in the recommended format for Hipparcos stars
2	RAdeg	deg	Right Ascension 2000 (degrees)
3	DEdeg	deg	Declination 2000 (degrees)
4	B	mag	Magnitude in Johnson B
5		mag	Error of Magnitude in Johnson B
6	V	mag	Magnitude in Johnson V
7		mag	Error of Magnitude in Johnson V
8	I	mag	Magnitude in Johnson I
9		mag	Error of Magnitude in Johnson I
10	J	mag	2MASS J-band magnitude
11		mag	Error of 2MASS J-band magnitude
12	H	mag	2MASS H-band magnitude
13		mag	Error of 2MASS H-band magnitude
14	K_s	mag	2MASS K-band magnitude
15		mag	Error of 2MASS K-band magnitude
16	[3.4]	mag	W1 magnitude of WISE
17		mag	Error of W1 magnitude of WISE
18	[4.6]	mag	W2 magnitude of WISE
19		mag	Error of W2 magnitude of WISE
20	[12]	mag	W3 magnitude of WISE
21		mag	Error of W3 magnitude of WISE
22	[22]	mag	W4 magnitude of WISE
23		mag	Error of W4 magnitude of WISE
24	$K_s - [22]$	mag	Criterion of searching for $22 \mu\text{m}$ excess stars
25		mag	Error of $K_s - [22]$
26	f_d	—	Fractional Luminosity
27	SpType	—	Spectral Type
28	Note	—	Notes for stars
29	Refs	—	Reference

6. Table of IR excess stars: The 140 Main-Sequence stars and 1 Giants

Table 3. Stars with 22 μm Excess

HIP	RAdeg (J2000)	DEdeg (J2000)	...	K_s (mag)	...	[12] (mag)	[22] (mag)	$K_s - [22]$ (mag)	f_d	SpType	Note	Refs				
301	0.93488485	-17.33597	...	4.56	0.02	...	4.52	0.01	4.23	0.02	0.34	0.03	3.47e-05	B9		
560	1.7084357	-23.107426	...	5.24	0.02	...	5.23	0.01	4.51	0.02	0.73	0.03	3.61e-04	F2		Rebull et al. (2008)
682	2.1070592	6.6168075	...	6.12	0.02	...	6.1	0.01	5.75	0.04	0.37	0.05	2.84e-04	G2	Disk	Moór et al. (2006)
813	2.5091026	11.145809	...	5.7	0.02	...	5.62	0.01	5.38	0.04	0.33	0.04	3.39e-05	B9	D or M	Simbad
2496	7.9197493	-1.7936332	...	6.89	0.02	...	6.78	0.02	5.8	0.04	1.08	0.04	3.25e-04	A0	C	
4366	13.993843	27.209354	...	5.75	0.02	...	5.75	0.01	5.29	0.03	0.45	0.04	1.17e-04	A5		
6507	20.895601	-24.352776	...	6.11	0.02	...	6.05	0.01	5.82	0.04	0.29	0.04	1.15e-04	A9	D or M	Simbad
6679	21.41935	2.972085	...	5.9	0.02	...	5.92	0.01	5.6	0.03	0.29	0.04	1.18e-04	F0	C; in Double system	
7345	23.657173	-15.6763525	...	5.46	0.02	...	5.34	0.01	3.74	0.02	1.72	0.03	1.54e-03	A1		Rhee et al. (2007)
7805	25.099968	-60.99904	...	6.63	0.02	...	6.6	0.01	6.05	0.04	0.58	0.04	2.56e-04	F2		Rhee et al. (2007)
7943	25.514395	35.245766	...	5.78	0.02	...	5.75	0.01	5.04	0.03	0.74	0.03	8.77e-05	B9		
8122	26.09486	32.51604	...	6.17	0.02	...	6.18	0.01	5.66	0.04	0.51	0.04	1.16e-04	A3		Rhee et al. (2007)
9570	30.74153	33.284153	...	5.33	0.02	...	5.34	0.01	5.06	0.03	0.27	0.03	6.04e-05	A2		Rhee et al. (2007)
10320	33.226917	-30.723843	...	5.21	0.02	...	5.08	0.01	4.66	0.03	0.54	0.03	9.37e-05	A0		
10670	34.328484	33.84732	...	3.96	0.03	...	3.98	0.01	3.51	0.02	0.45	0.03	8.20e-05	A1		Rhee et al. (2007)
11360	36.567474	6.292674	...	5.82	0.02	...	5.79	0.01	5.26	0.03	0.56	0.04	2.48e-04	F2	C;	Rhee et al. (2007)
11477	37.007042	-33.811054	...	4.94	0.03	...	4.98	0.01	4.56	0.02	0.38	0.03	7.80e-05	A2/A3		
11847	38.232403	37.33374	...	6.55	0.02	...	6.5	0.02	4.23	0.03	2.32	0.03	1.25e-02	F0		Rhee et al. (2007)
12351	39.75498	-58.18722	...	5.76	0.02	...	5.53	0.01	5.44	0.03	0.31	0.03	9.30e-04	M0		
12361	39.781216	-52.93493	...	5.92	0.03	...	5.9	0.01	5.43	0.03	0.49	0.04	1.83e-04	F0/F2	C;	Rhee et al. (2007)
13569	43.70644	-33.524895	...	6.22	0.02	...	6.21	0.01	5.87	0.03	0.34	0.04	7.79e-05	A3		
15039	48.45911	-38.809284	...	6.43	0.02	...	6.43	0.01	6.11	0.04	0.32	0.05	6.73e-05	A2/A3		
15933	51.303272	-37.15268	...	6.87	0.02	...	6.83	0.02	6.59	0.05	0.27	0.05	7.27e-05	A4		
16449	52.973385	-25.614113	...	6.1	0.02	...	6.11	0.01	5.39	0.03	0.71	0.04	1.82e-04	A3		Rhee et al. (2007)
16638	53.51848	-41.33871	...	6.67	0.02	...	6.63	0.01	6.41	0.04	0.26	0.04	1.24e-04	F2		
17395	55.890995	-10.485612	...	5.08	0.02	...	5.08	0.01	4.66	0.03	0.42	0.03	1.08e-04	A5	Disk	Gáspár et al. (2013)
17681	56.817085	44.07382	...	7.08	0.02	...	6.97	0.01	6.17	0.04	0.91	0.05	1.29e-04	B9		
18187	58.36331	-41.22287	...	5.98	0.02	...	5.95	0.01	5.64	0.03	0.33	0.04	1.81e-04	F6	IR excess	Mizusawa et al. (2012)
18437	59.122307	-38.96217	...	6.86	0.02	...	6.71	0.01	5.12	0.02	1.74	0.03	1.47e-03	A0		Rhee et al. (2007)
18671	59.975647	-54.161247	...	6.78	0.02	...	6.72	0.01	6.51	0.04	0.27	0.05	1.49e-04	F5		
20063	64.53372	42.141247	...	6.35	0.02	...	6.37	0.02	5.66	0.04	0.69	0.05	7.79e-05	B9		
20713	66.586136	15.618346	...	4.03	0.24	...	3.78	0.01	3.77	0.03	0.26	0.24	1.09e-04	F0		
20737	66.66073	-28.951828	...	6.74	0.02	...	6.7	0.01	6.34	0.05	0.4	0.05	4.15e-04	K0		
21020	67.611206	-43.212772	...	7.31	0.02	...	7.23	0.01	6.38	0.05	0.93	0.05	2.27e-04	A0		

Table 3—Continued

HIP	RAdeg (J2000)	DEdeg (J2000)	...	K_s (mag)	...	[12] (mag)	[22] (mag)	$K_s - [22]$ (mag)	f_d	SpType	Note	Refs				
21024	67.62306	-43.410667	...	7.22	0.02	...	7.09	0.02	5.54	0.03	1.68	0.04	1.27e-03	A0		
21038	67.66001	32.457813	...	6.2	0.02	...	6.19	0.02	5.9	0.04	0.29	0.05	3.15e-05	B9	Double?	
21618	69.6201	-19.640846	...	6.49	0.02	...	6.48	0.01	6.19	0.04	0.3	0.05	1.15e-04	A9		
21765	70.12219	-9.195834	...	6.27	0.02	...	6.07	0.01	5.96	0.05	0.31	0.05	9.15e-04	M0	Double?	
22226	71.706276	-26.302446	...	6.89	0.02	...	6.87	0.01	6.05	0.04	0.84	0.05	5.10e-04	F3		Rhee et al. (2007)
22531	72.730774	-53.46172	...	4.8	0.02	...	4.16	0.01	4.37	0.02	0.43	0.03	1.62e-04	F0	in Double system	Simbad
24528	78.93295	-22.894373	...	6.43	0.03	...	6.36	0.02	5.59	0.04	0.84	0.05	2.44e-04	A3		Rhee et al. (2007)
24947	80.15841	-39.754974	...	6.14	0.02	...	6.1	0.01	5.87	0.03	0.28	0.04	1.61e-04	F6	Disk	Zuckerman et al. (2011)
25183	80.801575	-31.748575	...	6.41	0.02	...	6.41	0.01	6.06	0.04	0.35	0.04	1.65e-04	F3	Binary; IR excess identified	Mizusawa et al. (2012)
25453	81.661766	6.8687367	...	6.44	0.02	...	6.32	0.02	4.79	0.03	1.65	0.04	1.20e-03	A0		
25517	81.85334	-26.584913	...	6.7	0.04	...	6.66	0.01	6.23	0.05	0.48	0.06	1.07e-04	A3	C	
25608	82.063866	-37.23093	...	5.5	0.02	...	5.52	0.01	5.22	0.03	0.28	0.03	5.10e-05	A0		
25998	83.23498	-47.689034	...	7.34	0.02	...	7.31	0.01	5.94	0.03	1.4	0.04	8.86e-04	A3	C	
26062	83.37814	24.628914	...	6.82	0.02	...	5.13	0.01	2.28	0.02	4.53	0.03	4.34e-01	B8		
26309	84.04282	-28.708006	...	5.86	0.02	...	5.8	0.01	5.06	0.03	0.8	0.03	2.04e-04	A2		
26453	84.41505	-28.626286	...	6.28	0.02	...	6.21	0.01	5.34	0.03	0.94	0.04	6.43e-04	F3	C;	Rhee et al. (2007)
26621	84.8769	-40.68407	...	7.1	0.02	...	7.02	0.01	6.41	0.04	0.69	0.05	6.28e-05	B8		
26796	85.362175	-33.40071	...	6.43	0.03	...	6.4	0.02	5.74	0.03	0.69	0.04	7.78e-05	B9	Excess at 24 μm	Morales et al. (2009)
26966	85.84025	-18.557444	...	5.78	0.03	...	5.63	0.02	4.57	0.03	1.22	0.04	4.43e-04	A0		Rhee et al. (2007)
26990	85.899124	-39.92357	...	6.76	0.02	...	6.72	0.01	6.39	0.04	0.37	0.05	2.50e-04	G0		
27259	86.67538	-36.23131	...	6.65	0.02	...	6.65	0.01	5.94	0.04	0.71	0.04	1.82e-04	A3		
28186	89.35313	-40.39784	...	6.86	0.02	...	6.79	0.01	6.63	0.05	0.23	0.05	1.34e-04	F5		
28230	89.46913	-34.47607	...	6.88	0.02	...	6.83	0.01	5.72	0.03	1.16	0.04	7.84e-04	A8		Rhee et al. (2007)
29888	94.4058	-24.444433	...	6.35	0.02	...	6.23	0.01	6.14	0.04	0.21	0.04	1.29e-04	F5	in Double system	Simbad
30174	95.234924	-29.67068	...	6.4	0.02	...	6.08	0.01	6.03	0.04	0.37	0.04	1.73e-04	F3	Eclipsing Binary	Simbad
31386	98.69566	-63.262104	...	7.05	0.02	...	7.02	0.01	6.74	0.04	0.31	0.05	9.71e-05	A7		
36624	112.98193	38.896122	...	6.42	0.02	...	6.4	0.02	5.84	0.04	0.57	0.05	1.20e-04	A2		
38403	118.01622	45.933098	...	6.02	0.02	...	6.03	0.01	5.67	0.04	0.35	0.04	7.90e-05	A3		
39535	121.18883	18.842068	...	6.28	0.02	...	6.31	0.01	5.91	0.05	0.36	0.05	3.71e-05	B9		
40415	123.7574	-79.318756	...	7.02	0.03	...	7.05	0.02	6.7	0.04	0.32	0.06	5.66e-05	A0		
41152	125.9522	53.21995	...	5.25	0.02	...	5.27	0.01	4.85	0.03	0.4	0.03	8.94e-05	A3		Rhee et al. (2007)
42197	129.06482	42.57988	...	6.5	0.02	...	6.5	0.02	6.1	0.05	0.4	0.05	8.02e-05	A2		
42753	130.69264	31.862701	...	6.21	0.02	...	5.82	0.02	5.74	0.04	0.47	0.04	2.82e-04	F8	Eclipsing Binary	Simbad
43121	131.73357	12.110076	...	5.55	0.02	...	5.56	0.01	5.06	0.03	0.49	0.04	9.12e-05	A1	Disk	Morales et al. (2009)

Table 3—Continued

HIP	RAdeg (J2000)	DEdeg (J2000)	...	K_s (mag)	...	[12] (mag)	[22] (mag)	$K_s - [22]$ (mag)	f_d	SpType	Note	Refs				
43970	134.31213	15.322718	...	4.87	0.02	...	4.92	0.01	4.6	0.03	0.27	0.03	7.65e-05	A5		Rhee et al. (2007)
46897	143.35873	-22.864017	...	5.8	0.02	...	5.85	0.01	5.53	0.04	0.27	0.04	2.96e-05	B9		
46919	143.44405	62.827904	...	5.21	0.02	...	5.05	0.01	4.94	0.03	0.27	0.03	2.46e-04	G5	Giant star	
47336	144.69057	10.777873	...	6.33	0.03	...	6.32	0.01	5.99	0.04	0.33	0.05	7.66e-05	A3	in Double system	Simbad
47522	145.32094	-23.591522	...	4.54	0.02	...	3.63	0.01	2.89	0.02	1.65	0.02	3.01e-04	B5	Be star with excess	Touhami et al. (2011)
48164	147.26195	34.08553	...	6.63	0.02	...	6.66	0.02	6.19	0.05	0.44	0.05	9.67e-05	A3		Rhee et al. (2007)
48541	148.49657	27.695465	...	7.19	0.02	...	7.1	0.02	6.1	0.04	1.1	0.05	3.36e-04	A0		Rhee et al. (2007)
49582	151.83284	-15.455298	...	7.25	0.03	...	7.14	0.01	6.23	0.04	1.02	0.06	6.29e-04	F0		
51259	157.0607	-36.220123	...	6.47	0.03	...	6.47	0.01	6.24	0.05	0.24	0.06	1.27e-04	F3		
53824	165.1868	6.1015034	...	4.61	0.02	...	4.6	0.01	4.26	0.03	0.35	0.03	9.31e-05	A5	in Double system	Simbad
55485	170.45563	57.074844	...	5.99	0.02	...	5.99	0.01	5.56	0.04	0.43	0.04	1.27e-04	A7		Morales et al. (2009)
55700	171.19781	-22.832798	...	6.69	0.02	...	6.69	0.01	6.41	0.05	0.29	0.05	9.21e-05	A7		
59422	182.84108	-3.7787178	...	5.91	0.02	...	5.93	0.01	5.52	0.04	0.39	0.05	1.95e-04	F5		
61281	188.37102	69.78821	...	3.82	0.04	...	2.6	0.01	1.82	0.01	2.0	0.04	8.14e-04	B6	Be star	Simbad
61558	189.19737	-5.831851	...	5.7	0.02	...	5.71	0.01	5.18	0.04	0.52	0.04	1.17e-04	A3		
61960	190.47087	10.235843	...	4.68	0.02	...	4.7	0.01	4.27	0.02	0.41	0.03	6.91e-05	A0		Rhee et al. (2007)
62576	192.32297	27.552326	...	5.62	0.02	...	5.65	0.02	5.28	0.03	0.33	0.04	6.93e-05	A2	in Double system	Simbad
63942	196.56429	20.728996	...	6.04	0.02	...	5.87	0.01	5.69	0.04	0.35	0.04	1.00e-03	M0	D or M	Simbad
64461	198.19316	34.528233	...	6.77	0.02	...	6.76	0.02	6.49	0.05	0.28	0.05	1.49e-04	F5		
64774	199.1194	68.40796	...	6.27	0.02	...	6.28	0.01	5.96	0.04	0.31	0.04	3.27e-05	B9		
67005	205.97832	52.064426	...	5.99	0.02	...	6.02	0.01	5.66	0.03	0.33	0.04	6.26e-05	A1		
67495	207.46844	13.191899	...	6.22	0.02	...	6.22	0.01	5.86	0.04	0.36	0.04	7.41e-05	A2		
67596	207.76878	34.772537	...	6.35	0.02	...	6.38	0.01	6.0	0.04	0.35	0.04	9.22e-05	A5		
67953	208.74294	-8.058764	...	5.08	0.03	...	4.89	0.01	4.87	0.03	0.21	0.04	1.54e-04	F8	in Double system	Simbad
69281	212.73259	15.215671	...	6.59	0.03	...	6.58	0.01	6.22	0.04	0.37	0.05	2.52e-04	G0	C; in Double system	Simbad
69917	214.62985	52.03333	...	6.56	0.02	...	6.56	0.01	6.23	0.04	0.33	0.04	6.79e-05	A2		
70386	216.02385	11.246967	...	6.07	0.02	...	5.15	0.01	5.58	0.03	0.49	0.04	2.43e-04	F5	in Double system	Simbad
71602	219.65645	54.853245	...	6.41	0.03	...	6.4	0.01	6.14	0.04	0.27	0.05	1.27e-04	F2		
72138	221.33464	-6.7345963	...	6.76	0.03	...	6.52	0.01	6.43	0.05	0.33	0.06	2.29e-04	G0	Eclipsing Binary	Simbad
72505	222.36974	19.510384	...	6.78	0.02	...	6.79	0.02	6.38	0.04	0.4	0.05	4.04e-05	B9	C	
72552	222.49327	28.615833	...	5.59	0.02	...	5.57	0.01	5.05	0.03	0.53	0.03	1.33e-04	A4	in Double system	Simbad
73730	226.07346	59.535053	...	6.99	0.02	...	6.96	0.01	6.63	0.05	0.36	0.05	7.36e-05	A2		
74553	228.497	43.04797	...	6.11	0.02	...	6.06	0.01	5.63	0.03	0.48	0.04	1.24e-04	A5		
75953	232.69203	34.465683	...	6.7	0.02	...	6.7	0.01	6.08	0.04	0.62	0.04	1.12e-04	A0		

Table 3—Continued

HIP	RAdeg (J2000)	DEdeg (J2000)	...	K_s (mag)	...	[12] (mag)	[22] (mag)	$K_s - [22]$ (mag)	f_d	SpType	Note	Refs				
76305	233.80867	65.27768	...	7.23	0.02	...	7.21	0.01	6.78	0.05	0.45	0.05	9.14e-05	A2	C	
76773	235.12596	37.017002	...	7.14	0.02	...	7.13	0.01	6.41	0.04	0.74	0.05	1.47e-04	A0		
77094	236.12613	3.3701653	...	6.31	0.03	...	6.29	0.01	5.98	0.04	0.32	0.05	1.66e-04	F5		
77163	236.34778	5.4473224	...	5.43	0.02	...	5.43	0.01	4.97	0.03	0.45	0.03	8.32e-05	A1		Rhee et al. (2007)
77986	238.87755	42.56615	...	5.85	0.01	...	5.65	0.01	4.99	0.02	0.86	0.03	1.16e-04	B9	Be Star	Simbad
78017	238.95691	58.91171	...	6.41	0.02	...	6.39	0.01	6.07	0.03	0.34	0.04	5.86e-05	A0		
80427	246.2511	51.716564	...	6.82	0.02	...	6.83	0.01	6.55	0.04	0.27	0.04	6.63e-05	A3		
81641	250.1612	4.219815	...	5.74	0.02	...	5.78	0.01	5.33	0.03	0.4	0.04	7.43e-05	A1		Rhee et al. (2007)
82587	253.24217	31.701715	...	4.56	0.02	...	4.53	0.01	4.3	0.03	0.26	0.03	1.09e-04	F0	C; in Double system	Simbad
84732	259.8121	79.305435	...	6.92	0.02	...	6.91	0.01	6.65	0.04	0.26	0.04	7.62e-05	A5		
85790	262.95657	28.407436	...	5.64	0.03	...	5.63	0.01	5.25	0.03	0.39	0.04	7.16e-05	A1	contamination	Rhee et al. (2007)
86446	264.94983	49.779842	...	6.58	0.02	...	6.57	0.01	6.25	0.04	0.33	0.04	5.78e-05	A0		
87944	269.48572	43.417114	...	6.86	0.02	...	6.88	0.01	6.49	0.04	0.37	0.05	3.72e-05	B9		
88349	270.62814	58.62721	...	6.58	0.03	...	6.58	0.01	6.13	0.04	0.45	0.04	9.10e-05	A2		
92676	283.25986	-48.360725	...	5.85	0.02	...	5.8	0.02	5.2	0.03	0.65	0.04	1.43e-04	A2		↑
93542	285.77847	-42.094994	...	4.75	0.02	...	4.72	0.01	3.79	0.03	0.96	0.03	2.44e-04	A0		Rhee et al. (2007)
94140	287.44083	65.97845	...	6.26	0.02	...	6.19	0.01	5.45	0.03	0.81	0.03	1.72e-04	A0		
95261	290.71326	-54.42373	...	5.01	0.03	...	4.73	0.01	3.25	0.02	1.76	0.04	1.53e-03	A0		Rhee et al. (2007)
95270	290.74548	-54.53785	...	5.91	0.03	...	5.89	0.01	3.96	0.02	1.95	0.04	7.10e-03	F5/F6		Rhee et al. (2007)
99892	304.01157	-16.295567	...	6.72	0.02	...	6.68	0.02	5.93	0.05	0.79	0.05	1.67e-04	A0		
100787	306.5198	-46.659958	...	6.15	0.02	...	6.12	0.01	5.77	0.04	0.38	0.05	1.38e-04	A9		
102419	311.31223	-15.79827	...	6.12	0.03	...	6.14	0.02	5.8	0.05	0.33	0.05	1.43e-04	F2/F3		
103048	313.17328	-53.273277	...	6.56	0.02	...	6.54	0.01	6.05	0.05	0.51	0.05	2.56e-04	F5/F6		
105169	319.5675	-75.346664	...	6.54	0.02	...	6.55	0.01	6.05	0.04	0.49	0.05	8.97e-05	A1		
106741	324.33783	-18.440924	...	6.18	0.02	...	6.18	0.01	5.93	0.05	0.25	0.05	1.31e-04	F3/F5		Rhee et al. (2007)
106783	324.4317	6.6183963	...	6.11	0.02	...	6.13	0.01	5.77	0.04	0.34	0.04	7.08e-05	A2	in Double system	Simbad
107336	326.0995	-4.730885	...	6.41	0.02	...	6.39	0.02	6.13	0.05	0.28	0.05	6.15e-05	A2		
107585	326.8533	-4.6086183	...	6.68	0.02	...	6.64	0.02	5.77	0.05	0.91	0.05	2.62e-04	A2		
107596	326.90918	-5.91684	...	5.63	0.03	...	5.62	0.01	5.22	0.04	0.41	0.05	1.22e-04	A7		
107919	327.9661	11.091197	...	6.05	0.03	...	6.07	0.01	5.55	0.04	0.5	0.05	1.31e-04	A5		
109230	331.9346	-28.147606	...	6.47	0.03	...	6.49	0.02	6.2	0.05	0.27	0.05	1.12e-04	Fm		
110739	336.52835	-5.1778803	...	6.56	0.02	...	6.55	0.02	6.14	0.05	0.41	0.05	1.55e-04	F0		
110786	336.67352	-11.22817	...	6.32	0.02	...	6.34	0.01	5.83	0.05	0.49	0.05	1.10e-04	A3		
112542	341.92813	-14.056405	...	5.73	0.02	...	5.74	0.01	5.15	0.03	0.58	0.04	6.09e-05	B9	in Double system	Simbad

Table 3—Continued

HIP	RAdeg (J2000)	DEdeg (J2000)	...	K_s (mag)	...	[12] (mag)	[22] (mag)	$K_s - [22]$ (mag)	f_d	SpType	Note	Refs				
114822	348.89276	-3.4963725	...	5.4	0.02	...	5.43	0.01	5.1	0.03	0.31	0.04	7.17e-05	A3		
116431	353.90048	8.382718	...	6.4	0.02	...	6.41	0.01	5.01	0.03	1.4	0.04	1.49e-03	F0		Rhee et al. (2007)
117481	357.33157	-27.854132	...	5.7	0.03	...	5.71	0.01	5.44	0.04	0.26	0.05	1.54e-04	F6/F7		
118133	359.4425	11.4744005	...	6.59	0.02	...	6.58	0.02	6.11	0.05	0.48	0.05	4.87e-05	B9	in Double system	Simbad
118322	359.9788	-65.57708	...	4.6	0.02	...	4.57	0.01	4.31	0.02	0.29	0.03	3.13e-05	B9	Be Star	Simbad

Note. — C: Contaminated stars from W4 band images;
D or M: Double or multiple star;
Disk: IR excess stars with disk;
Double?: May be the double system;
The editor can get the full version of this Table from author.

Table 4. $22\ \mu\text{m}$ Excess Detect rate of Main-Sequence Stars

SpType	Detection	Total
B	20	120
A	76	617
F	36	1220
G	4	531
K	1	142
M	3	19

Note. — The total number only contains those with W4 $S/N \geq 20$ and low IRAS $100\ \mu\text{m}$ background level.

A. Gallery of images and SEDs (The first 3 stars)

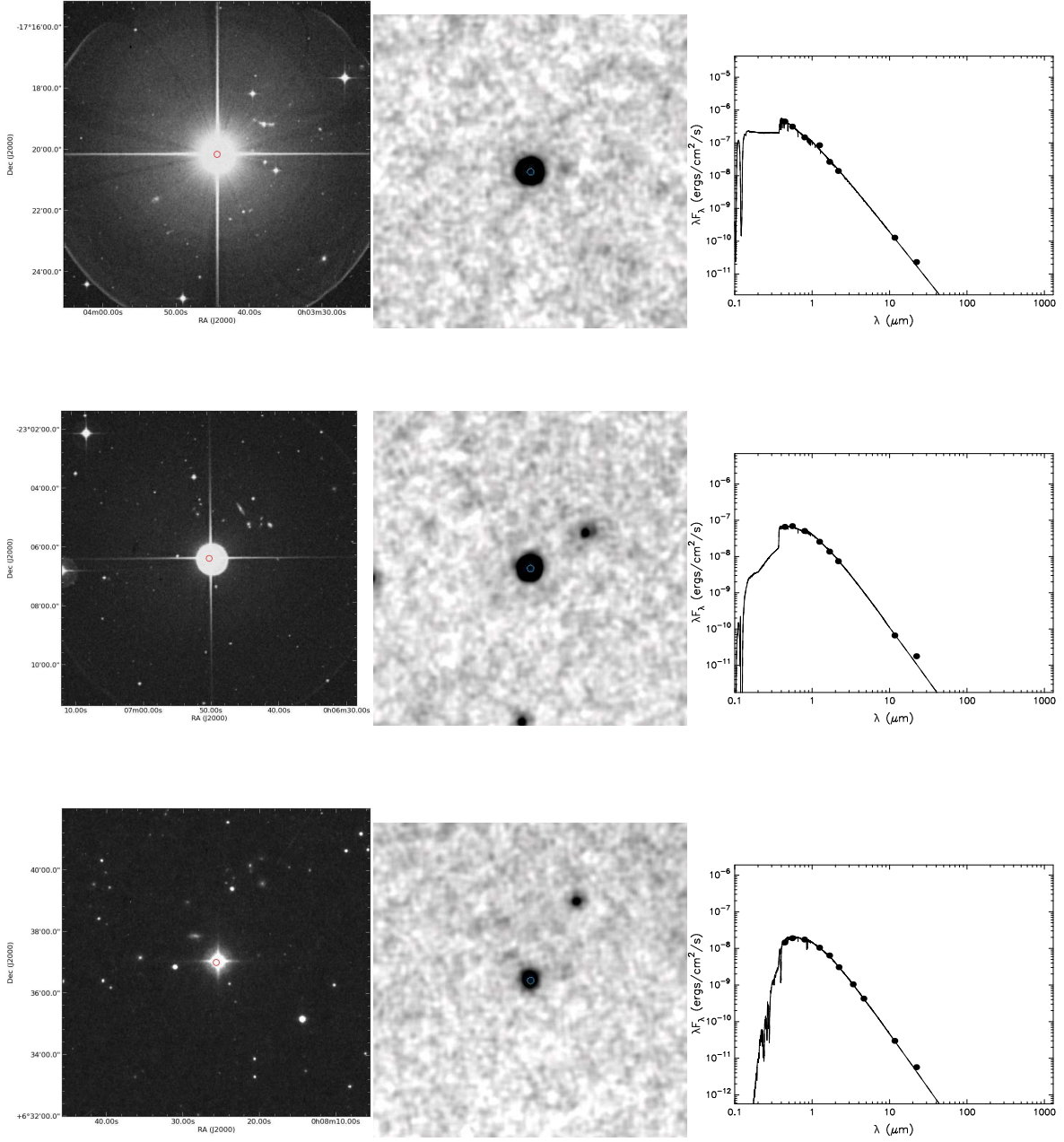


Fig. 16.— The optical images and SEDs of the first 3 stars. From top to bottom, the name of stars are hip301, hip560, hip682, respectively. The editor can get the full version of this gallery from author.